RATE OPTIMIZATION FOR POLYMER AND CO_2 FLOODING UNDER GEOLOGIC UNCERTAINTY

A Thesis

by

MOHAN SHARMA

Submitted to the Office of Graduate Studies of
Texas A&M University
in partial fulfillment of the requirements for the degree of

MASTER OF SCIENCE

August 2011

Major Subject: Petroleum Engineering

Rate Optimization for Polymer and CO_2 Flooding

Under Geologic Uncertainty

RATE OPTIMIZATION FOR POLYMER AND CO_2 FLOODING

UNDER GEOLOGIC UNCERTAINTY

A Thesis

by

MOHAN SHARMA

Submitted to the Office of Graduate Studies of
Texas A&M University
in partial fulfillment of the requirements for the degree of

MASTER OF SCIENCE

Approved by:

Co-Chairs of Committee,	Akhil Datta-Gupta
	Michael King
Committee Member,	Wolfgang Bangerth
Head of Department,	Stephen A. Holditch

August 2011

Major Subject: Petroleum Engineering

ABSTRACT

Rate Optimization for Polymer and CO_2 Flooding
Under Geologic Uncertainty. (August 2011)
Mohan Sharma, B.S., Indian School of Mines, Dhanbad, India
Co-Chairs of Advisory Committee: Dr. Akhil Datta-Gupta
Dr. Michael King

With the depletion of the existing reservoirs and the decline in oil discoveries during the last few decades, enhanced oil recovery (EOR) methods have gained a lot of attention. Among the various improved recovery methods, waterflooding is by far the most widely used. However, the presence of reservoir heterogeneity such as high permeability streaks often leads to premature breakthrough and poor sweep resulting in reduced oil recovery. This underscores the need for prudent reservoir management, in terms of optimal production and injection rates, to maximize recovery. The increasing deployment of smart well completions and i-field has inspired many researchers to develop algorithms to optimize the production/injection rates along intervals of smart wells. However, the application of rate control for other EOR methods has been relatively few.

This research aims to extend previous streamline-based rate optimization workflow to polymer flooding and CO_2 flooding. The objective of the approach is to maximize sweep efficiency and minimize recycling of injected fluid (polymer/CO_2) by delaying its breakthrough. This is achieved by equalizing the front arrival time at the producers using streamline time-of-flight. Arrival time is rescaled to allow for optimization after breakthrough of injected fluid. Additionally, we propose an accelerated production strategy to increase NPV over sweep efficiency maximization case. The optimization is performed under operational and facility constraints using a sequential quadratic programming approach. The geological uncertainty has been

accounted for via a stochastic optimization framework based on the combination of the expected value and variance of a performance measure from multiple realizations.

Synthetic and field examples are used extensively to demonstrate the practical feasibility and robustness of our approach for application to EOR processes.

DEDICATION

To my parents for their love, care and support

ACKNOWLEDGEMENTS

I would like to thank my committee co-chairs, Dr. Akhil Datta-Gupta and Dr. Michael King for their valuable guidance and financial support throughout the course of this research. Also I want to thank my committee member, Dr. Bangerth for his valuable feedback and questions that have shaped the work in this research.

Thanks to my colleagues in the MCERI research group for the constructive discussions and their friendship. Especially, I want to acknowledge Satyajit and Alvaro for all the valuable inputs through the different stages of my work.

TABLE OF CONTENTS

CHAPTER Page

LIST OF FIGURES

FIGURE Page

FIGURE Page

CHAPTER I

INTRODUCTION

Since most of the current world oil production comes from mature fields, increasing ultimate oil recovery from these fields is critical to meet the growing energy demand in the coming years. Among the various improved recovery methods waterflooding is by far the most widely used (Lake et al. 1992; Craig 1993). Waterfloods are relatively inexpensive and easy to implement. However, the presence of reservoir heterogeneity such as high permeability streaks often leads to premature breakthrough and poor sweep, resulting in reduced oil recovery. This underscores the need for a prudent reservoir management in terms of optimal production and injection rates, to maximize recovery during waterflood.

It is well recognized that field-scale rate optimization problems often involve highly complex reservoir model, production and facility related constraints and geological uncertainty. Deployment of smart well completions with inflow control valves (ICV) to control production/injection rates for various segments along the wellbore further compounds to the complexity of the optimization. All these make optimal reservoir management via rate control difficult without efficient optimization algorithms. Two main types of optimization algorithms have been developed to address the problem, namely gradient-based algorithms and stochastic algorithms (Brouwer and Jansen 2004; Tavakkolian et al. 2004). Both algorithms use reservoir simulators to evaluate the objective function. The gradient-based algorithms require an estimation of the gradient of the objective function with respect to the control variables. In contrast, the stochastic algorithms such as the genetic algorithm do not require estimation of the gradient but typically require multiple forward simulations for evaluations of the objective function or an appropriately defined fitness function. The advantage of

---

This dissertation follows the style of *SPE Reservoir Evaluation & Engineering.*

stochastic optimization is the ability to search for a global solution while the gradient-based optimizations typically search for a local solution. The disadvantage of the stochastic optimization is the extensive computational power requirement especially when the number of control variables is large.

Alhuthali et al. (2007; 2008; 2010) proposed a streamline-based approach to maximize waterflood sweep efficiency, which focused on equalizing arrival time of the waterfront at all producers within selected sub-regions of a waterflood project. This resulted in delayed water breakthrough and reduced field water cut after water breakthrough. The optimization was performed under operational and facility constraints using a sequential quadratic programming approach. A major advantage of the streamline-based approach is the analytical computation of the sensitivities of the waterfront arrival times at the producers to well production/injection rates and the gradient and Hessian of the objective function. This makes it computationally efficient and suitable for large field cases. Alhuthali et al. (2008) accounted for geological uncertainty via a stochastic optimization framework based on the combination of the expected value and variance of a performance measure from multiple realizations.

This approach however, has a drawback that it solely focuses on maximizing sweep efficiency, and not necessarily the NPV. To address this issue, the objective function was redefined by adding 'norm' penalty term to the objective function (Taware et al. 2010). Unlike the prior work of Alhuthali et al. (2010), the objective function now consists of two terms. The first term attempts to maximize the sweep efficiency while the second term attempts to accelerate the production. The trade-off between equalizing arrival time (maximizing sweep) and production acceleration (maximizing NPV) can be examined by adjusting the weight on the 'norm' penalty term. The optimal decision is a compromise between the two and can be arrived at by using a trade-off curve (Taware et al. 2010).

It is well known that waterflooding often results in poor sweep efficiency as injected water preferentially flows through high permeability zones, resulting in bypassed oil. Water soluble polymers are thus used to control mobility, leading to a more efficient sweep during waterflood, by attaining a close match of injectant viscosity to that of the in situ oil (Lake et al. 1992). However, the complexities and challenges associated with designing an optimal polymerflood need to be addressed for field-scale application. Similarly, carbon dioxide (CO_2) has been successfully used as EOR agent for decades because of its favorable properties of swelling oil, reducing oil viscosity and reducing residual oil saturation (Holm and Josendal 1974; Stalkup 1983). However, despite its high local displacement efficiency, the process has poor sweep efficiency due to viscous fingering caused by unfavorable mobility ratio and gravity segregation caused by density difference between injected and displaced phases (Christie and Bond 1987).

Issues long recognized for successful polymerflood like optimal selection of polymer type, concentration and slug size have been addressed by several authors (Kaminsky et al. 2007; Wang et al. 2008). Similarly, the design parameters influencing the sweep efficiency during CO_2 flood have been discussed by several authors (Green and Willhite 1998; Jarrell et al. 2002). However, guidelines for selection of optimal well production/injection rates during polymerflood and CO_2 flood still remain to be established and are addressed in this research.

1.1 Rate Optimization for Waterflooding Under Geologic Uncertainty

Streamline-based optimal reservoir management has shown great potential in maximizing sweep and reducing water recycling during waterflooding. It has been demonstrated by field application (Alhuthali et al. 2010) that sweep efficiency can be improved by appropriate allocation of production and injection rates. In this section we discuss the approach and mathematical formulation behind the existing streamline-based rate optimization workflow (Taware et al. 2010).

1.1.1 Approach

The primary objective of the approach is to obtain an optimal as well as accelerated production strategy for waterflooding based upon a trade-off between maximizing sweep efficiency and maximizing NPV. The approach is general and can be employed using both finite-difference and streamline models. Following are the steps involved in our approach:

- **Flow Simulation and streamline tracing.** The first step is to perform waterflood simulation for a time interval of interest for every geologic realization and compute the streamlines and time-of-flight from injectors to producers (Datta-Gupta and King 2007).

- **Computation of the objective function, analytical sensitivities and the Jacobian.** The second step is to compute the objective function for optimization which consists of two terms. The first term is the waterfront arrival time residuals which quantify the misfit between the desired arrival time and the computed arrival time at each producer for every geologic realization. The second term is a penalty term that minimizes the ‘norm’ (magnitude) of the arrival time itself to accelerate fluid production. Using streamlines, we compute the analytical sensitivities, which are defined as the partial derivatives of arrival time with respect to well rates. It should be noted that only one simulation run is required per realization in our approach to compute the sensitivities. The sensitivities are then used to compute the Jacobian which is defined as the gradient of the residuals.

- **Computation of analytical gradient and Hessian.** The next step is to compute the gradient and Hessian of the objective function using above computed residuals and the analytical Jacobian.

- **Minimization and optimal rate allocation.** The objective function is then minimized using Sequential Quadratic Programming (SQP) technique (Nocedal and Wright 2006) to generate required changes in rates subject to appropriate field constraints.

The above-mentioned steps are repeated for the time interval of interest, until a pre-defined stopping criterion on the objective function or the rates is satisfied. We then move to the next time interval for optimization.

1.1.2 Mathematical Formulation

In this section, we discuss the underlying formulation behind the optimization approach to derive optimal production/injection rates that attempt to maximize waterflood sweep efficiency as well as the NPV via production acceleration.

• **Objective Function Formulation**. The objective function consists of following two terms (Taware et al. 2010):

$$p(\mathbf{q}) = \sum_{m=1}^{N_{group}} \sum_{i=1}^{Nprod,m} \left(t_{d,m}(\mathbf{q}) - t_{i,m}(\mathbf{q})\right)^2 + \eta \sum_{m=1}^{N_{group}} \sum_{i=1}^{Nprod,m} \left(t_{i,m}(\mathbf{q})\right)^2 \quad \text{......................... (1.1)}$$

which can be expressed as:

$$p(\mathbf{q}) = \mathbf{e}_z^T \mathbf{e}_z + \eta\, \mathbf{t}_z^T \mathbf{t}_z \quad \text{.. (1.2)}$$

where the variable $t_{i,m}$ represents the calculated arrival time at well i, belonging to group m. The desired arrival time $t_{d,m}$ for the well group m is given by the arithmetic average of $t_{i,m}$, during each optimization iteration (Alhuthali et al. 2010). The vector $\mathbf{q}$ contains the control variables and has a dimension of n, the number of well rates to be optimized. In the present formulation of the objective function, the first term is expressed as the square of the l_2-norm of the arrival time residuals for a single geologic realization z. Minimization of this term ensures that the flood front arrives nearly at the same time for all producers in a given group of producers and injectors within the field. This results in maximizing sweep efficiency (Sudaryanto and Yortsos 2001; Alhuthali et al. 2007; 2008; 2010). The second term, which is the 'norm' penalty term, ensures that the magnitude of the arrival time is also reduced along with their variance. This reduction in arrival time leads to acceleration of production/injection and thus ensures that the optimization doesn't penalize highly productive wells too much in an attempt to improve sweep. By adjusting the weight η on the penalty term, we can decide on the trade-off between equalizing arrival time and accelerating production/injection. The optimal norm weight can be decided based upon a trade-off curve where the cumulative NPV (normalized to unity) is plotted against the norm weight. This gives a well-defined inflection point beyond which, for higher norm weights, the incremental benefit in NPV is small (Taware et al. 2010). Because of the trade-off between sweep efficiency and NPV, the inflection point can be considered to be the best compromise between the two. The approach retains the advantages of our approach viz. the analytical computation of the gradient and Hessian of the objective function using streamline-derived sensitivities. The derivation of the analytic gradient and Hessian follows the steps outlined by Alhuthali et al. (2008).

• **Optimization after breakthrough.** Since we have formulated our optimization in terms of arrival time of the water front at the producers, a natural question arises that what happens after water breakthrough. The optimization is carried out after water breakthrough at a well by incorporating the well water cut into the objective function so as to prevent allocating high production rates to wells with high water cut. To accomplish this, the arrival time to a well is modified to include the water cut at the well as:

$$t'_{i,m}(\mathbf{q}) = t_{i,m}(\mathbf{q}) * \left(1 - f_{w\,i,m}\right)^{\alpha} \quad \text{...} (1.3)$$

In the above expression, the arrival time, $t_{i,m}$, at well i belonging to group m has been altered to incorporate the well water cut, $f_{w\ i,m}$. If the water cut is zero, the modified arrival time is the same as the original arrival time. When the water cut at the well is greater than zero, the original arrival time will be rescaled based on the level of water cut. The extent of reduction can be controlled by the exponent term α. As a consequence, the rate allocation to the well will be lowered in relation to the wells with less water cut.

• **Accounting for Geologic Uncertainty.** To address geological uncertainty, **Eq. 1.2** needs to be generalized to handle multiple realizations. This is accomplished in terms of an expected value of the misfit in Eq. 1.2 for multiple realizations penalized by its standard deviation.

$$f(\mathbf{q}) = E[p(\mathbf{q})] + r\sigma[p(\mathbf{q})] \quad \text{..........} \quad (1.4)$$

Eq. 1.4 can be derived within the decision analysis framework (Alhuthali et al. 2010). The variable r is the risk coefficient that weights the trade-off between the expected value and the standard deviation. A positive r means that the decision maker is risk averse, while a negative r means that the decision maker is risk prone.

• **Objective Function Minimization.** The optimal rate allocation to producer/injector now involves the minimization of the penalized misfit function in Eq. 1.4. For field applications, the minimization must be carried out such that the production and facility constraints are acknowledged. Mathematically, this problem can be posed as follows:

$$\min_{\mathbf{q}} \; f(\mathbf{q})$$

Subject to

$$\mathbf{h}(\mathbf{q}) = 0$$
$$\mathbf{g}(\mathbf{q}) \le 0$$

Where $h : \Re^n \to \Re^z$ and $g : \Re^n \to \Re^y$ .... (1.5)

The vector **q** contains the control variables and has a dimension of *n*, the number of well rates to be optimized. The expressions **h(q)** and **g(q)** represent the equality and inequality constraints. In our approach, **Eq. 1.5** is minimized using the Sequential Quadratic Programming (SQP) algorithm for nonlinear constrained optimization (Nocedal and Wright 2006). The problem is formulated into a series of quadratic programming (QP) sub-problems which can be solved at each major iteration *k*. The QP sub-problem is mainly a quadratic approximation of the Lagrangian of Eq. 1.5 which is given in the following form:

$$L(\mathbf{q}, \boldsymbol{\lambda}_L, \boldsymbol{\lambda}_K) = f(\mathbf{q}) + \boldsymbol{\lambda}_L^T \mathbf{h}(\mathbf{q}) + \boldsymbol{\lambda}_K^T \mathbf{g}(\mathbf{q}) \qquad \text{(1.6)}$$

The vectors $\boldsymbol{\lambda}_\mathbf{L}$ and $\boldsymbol{\lambda}_\mathbf{K}$ refer to the Lagrange multipliers corresponding to the equality constraints and the Karush-Kuhn-Tucker multipliers corresponding to the inequality constraints. After linearizing the constraints using a Taylor approximation, the QP sub-problem can be written as:

$$\min_{\delta\mathbf{q}} \; f(\mathbf{q}^k) + \nabla_q f^T(\mathbf{q}^k)\delta\mathbf{q} + \frac{1}{2}\delta\mathbf{q}\nabla_q^2 L(\mathbf{q}^k)\delta\mathbf{q}$$

Subject to

$$\mathbf{h}(\mathbf{q}^k) + \nabla_q \mathbf{h}(\mathbf{q}^k)^T \delta\mathbf{q} = 0$$
$$\mathbf{g}(\mathbf{q}^k) + \nabla_q \mathbf{g}(\mathbf{q}^k)^T \delta\mathbf{q} \le 0 \qquad \text{(1.7)}$$

Details on formulating the QP sub-problem can be found in the previous work (Alhuthali et al. 2007). In our application, we have used the SQP algorithm

(MATLAB®) to obtain optimal rates for the nonlinear constrained optimization problem.

1.2 Objectives

The main objective of this research is to identify the applicability of the streamline-based rate optimization workflow described earlier for EOR methods. Specifically, the approach would be extended to polymer flooding and CO_2 flooding with modification for breakthrough at producers to improve sweep by equalizing flood front arrival time at multiple producers. We trace streamlines using the fluid fluxes derived from the finite-difference flow simulation. The streamlines are then used to analytically compute the sensitivities and the gradient and Hessian of the objective function. The hierarchy of rate and pressure constraints is captured during optimization through comprehensive constraint matrices. The objective function is then minimized using SQP technique to generate required changes in rates subject to specified field constraints. Moreover, we account for geologic uncertainty using multiple realizations via a stochastic optimization framework. In brief, we discuss the following:

- We will demonstrate that the approach provides optimal production/injection rates for polymer flooding and CO_2 flooding, using 2D heterogeneous example and cross section respectively.
- We will use field-scale cases to demonstrate the potential and practical viability of our approach for polymer flooding and CO_2 flooding.
- We will illustrate the robustness of our approach for polymer flooding and CO_2 flooding using multiple models to address geological uncertainty.

CHAPTER II

OPTIMAL POLYMERFLOOD MANAGEMENT VIA RATE CONTROL*

Waterflooding often results in poor sweep efficiency as injected water preferentially flows through high permeability zones resulting in bypassed oil. Water soluble polymers are thus used to control mobility, leading to a more efficient sweep during waterflood, by attaining a close match of injectant viscosity to that of the in situ oil (Lake et al. 1992).

The ongoing pilots and medium-scale polymerfloods presented by Moritis (2008) validate the EOR potential of this recovery process. However, its field-scale application has not been widespread because of complexities and challenges associated with designing an optimal polymerflood. If polymerflood is found techno-economically suitable for a reservoir after the pilot studies, the field-wide implementation requires optimal selection of polymer type, polymer solution viscosity, polymer concentration, polymer slug size and injection rate. Issues long recognized for successful polymerflood like optimal selection of polymer type, concentration and slug size have been addressed by several authors (Kaminsky et al. 2007; Wang et al. 2008). However, guidelines for selection of optimal well production/injection rates during polymerflood still remain to be established.

In this chapter, we extend the role of rate optimization for polymerflooding to maximize sweep efficiency and minimize polymer recycling by delaying polymer breakthrough. First, we outline the details of polymerflood modeling considered for our work. Then, we discuss the modification made to the approach (Taware et al. 2010).

* Part of this chapter is reprinted with permission from “Optimizing Polymerflood via Rate Control” by Sharma, M., Taware, S. and Datta-Gupta, A. 2011. Paper SPE 144833 presented at the 2011 SPE EOR Conference, Kuala Lumpur, Malaysia, 19-21 July. Copyright 2011 by the Society of Petroleum Engineers.

Finally, we demonstrate the robustness and application of our approach using a 2D heterogeneous example and a field-scale application.

2.1 Polymerflood Modeling

Displacement of viscous oil with water during waterflooding often results in poor areal sweep and viscous fingering due to adverse mobility ratio. Polymer injection during waterflooding of oil reservoirs decreases the mobility of the injected water (Lake 1989; Green and Willhite 1998). The reduction in mobility is caused by an increase in the water viscosity and a decrease in the rock permeability to water. The permeability to oil, however, remains largely unaffected. Both effects combine to reduce the water mobility which results in a more favorable fractional flow curve for the injected water, leading to more efficient areal sweep and reduced viscous fingering.

The commercial polymers can be broadly divided into two categories (Sorbie 1991): polyacrylamides (synthetic polymers) and polysaccharides (biopolymers). Polyacrylamides are polymers whose monomeric unit is the acrylamide molecule. Partially hydrolyzed polyacrylamides (HPAM) are used for field applications. The hydrolysis causes negatively charged carboxyl groups (—COO–) to be scattered along the backbone chain, which accounts for its physical properties. However, polyacrylamides are sensitive to brine salinity and shear stress. On the other hand, polysaccharides are formed from the polymerization of saccharide molecules through a bacterial fermentation process. Polysaccharides are insensitive to brine salinity and can tolerate mechanical shearing effects. However, it is susceptible to bacterial attack after it has been introduced into the reservoir.

In this study, we used a commercial simulator (ECLIPSE©) to model the physic-chemical aspects of polymerflooding. The general properties of polymer solution used here, representative of an HPAM solution, are given below:

2.1.1 Polymer Viscosity

The main property of interest during polymerflooding is the solution viscosity, which arises through molecular interactions among long polymer chains. The viscosity of a polymer solution is a function of polymer concentration and molecular weight. **Fig. 2.1** shows the variation in viscosity with polymer concentration used for our studies. The viscosity displayed here does not include shear thinning effect and is discussed later.

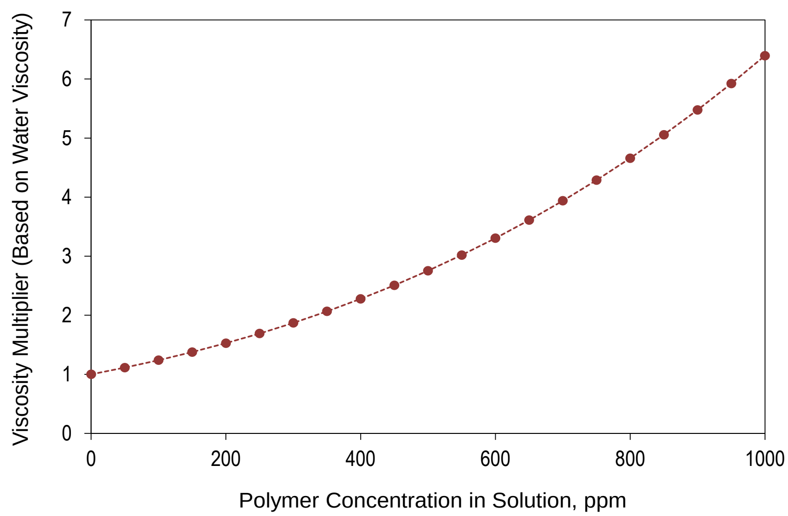

Fig. 2.1—Polymer solution viscosity (no shear thinning) vs. polymer concentration.

2.1.2 Polymer Retention

Polymer is retained by the porous media at the leading edge of the polymer slug which results in the formation of a stripped water bank ahead of the polymer front (Lake 1989; Sorbie 1991; Green and Willhite 1998). This water bank has mobility lower than the injected polymer solution and thus reduces the efficiency of polymerflood.

The three main retention mechanisms involved during polymerflood are polymer adsorption, mechanical entrapment and hydrodynamic retention. Adsorption occurs because of the interactions between the long chain polymer molecules and the rock surface, as a result of which molecules bound physically to the rock surface. Retention by mechanical entrapment occurs when some of the large molecules become lodged at the entrance to small pore throats. This retention mechanism is used as screening criteria for polymer selection and should be avoided. Hydrodynamic retention of polymer occurs when the fluid flow rate is adjusted to a new value resulting in changes in the steady state flow established earlier. This mechanism is reversible because almost the entire polymer is recovered by bringing rates to the original level. Moreover, hydrodynamic retention is not a very large contributor to the overall levels of polymer retention in field-scale polymerfloods. We used an adsorption isotherm as shown in **Fig. 2.2** for our studies.

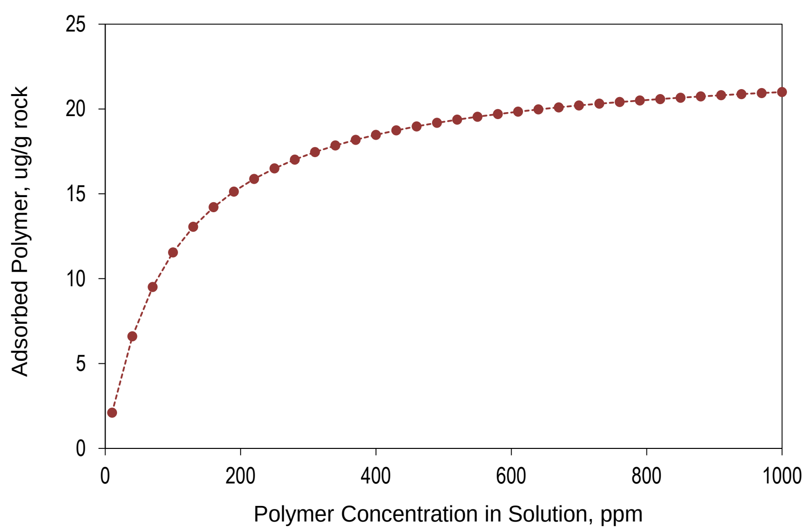

Fig. 2.2—Polymer adsorption vs. polymer concentration.

2.1.3 Permeability Reduction

A further effect caused by the adsorption and mechanical entrapment is a reduction in the rock permeability to the aqueous phase. Permeability reduction depends on the type of polymer and is directly correlated to the polymer concentration.

Permeability reduction is determined by first flooding a porous media with polymer solution and then completely displacing the polymer with brine. Residual resistance factor (RRF) is used to describe permeability reduction, which is defined as the ratio of the brine mobility before contact with polymer to the brine mobility after all mobile polymer has been displaced. We considered RRF equal to 3 for our studies.

2.1.4 Inaccessible Pore Volume

Because of large polymer molecule size, a portion of total pore space within the reservoir is inaccessible. This causes the polymer solution to travel at a faster velocity and thus counters the delay caused by polymer retention. We considered 20% pore volume to be inaccessible for our studies.

2.1.5 Non-Newtonian Rheology

Polymer solution, unlike water, does not show the same viscosity at all flow rates. At low flow rates the viscosity of the solution is approximately constant and depends only on the concentration of polymer in the solution. With increase in the flow rates, the solution viscosity reduces in a reversible manner. However, at even higher rates the large polymer molecules begin to break up and the viscosity approaches a limiting value not much greater than water viscosity. The effects tend to be greatest in the vicinity of injection wells where the fluid velocity is greatest, and so is the shear rate. We modeled non-Newtonian rheology **(Fig. 2.3)** by specifying a factor by which the polymer solution viscosity reduces corresponding to increasing water phase flow velocity (ECLIPSE©).

2.2 Polymerflood Rate Optimization

The streamline-based rate optimization approach discussed earlier is used to obtain an optimal as well as accelerated production strategy for polymerflooding. We trace streamlines using the fluid fluxes derived from the finite-difference flow simulation (Jimenez et al. 2008). The primary objective during sweep efficiency maximization is to equalize arrival time of water and polymer fronts at all producers within selected sub-regions of a polymerflood project. Additionally, accelerated production strategies were obtained by using norm weight with an objective to increase NPV. The geologic uncertainty is accounted using a stochastic framework for multiple realizations.

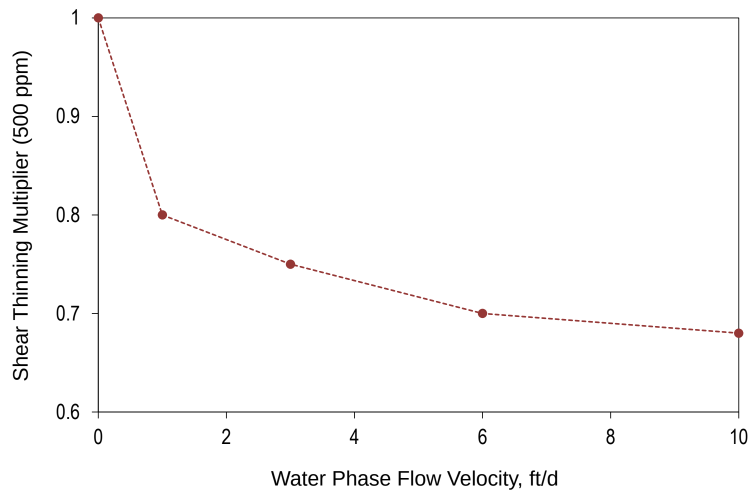

Fig. 2.3—Shear thinning with flow at 500 ppm polymer concentration.

2.2.1 Optimization After Polymer Breakthrough

Since we have formulated our optimization in terms of arrival time of the water and polymer fronts at the producers, a natural question arises that what happens after water and polymer breakthrough. The optimization is carried out after water breakthrough at a well by incorporating the well water cut into the objective function as described earlier in Eq. 1.3. A similar modification is done to the arrival time after polymer breakthrough for produced polymer concentration at the well as follows:

$$t''_{i,m}(\mathbf{q}) = t'_{i,m}(\mathbf{q}) * \left(1 - f_{pol\,i,m}\right)^{\alpha} \quad \text{(2.1)}$$

where

$$f_{pol\,i,m} = \frac{\text{Polymer produced at well (conc.)}}{\text{Max allowable polymer production at well (conc.)}} \quad \ldots\ldots\ldots\ldots\ldots\ldots\ldots\ldots\ldots (2.2)$$

Thus after polymer breakthrough, the arrival time is further rescaled based on fraction of produced polymer at the well w.r.t maximum allowable polymer production at that well ($f_{pol\ i,m}$). As a consequence, the rate allocation to the well will be lowered in relation to the wells with less polymer production. The well is shut when the produced polymer concentration reaches the maximum limit.

2.3 Illustration of the Approach

In this section, we illustrate our approach for five-spot polymerflooding in a 2D heterogeneous example. We first illustrate the benefits of polymerflooding over waterflooding for the base case. Then we demonstrate the application of our approach for maximizing sweep efficiency and production acceleration during polymerflooding using incremental oil recovery and reduced polymer recycling.

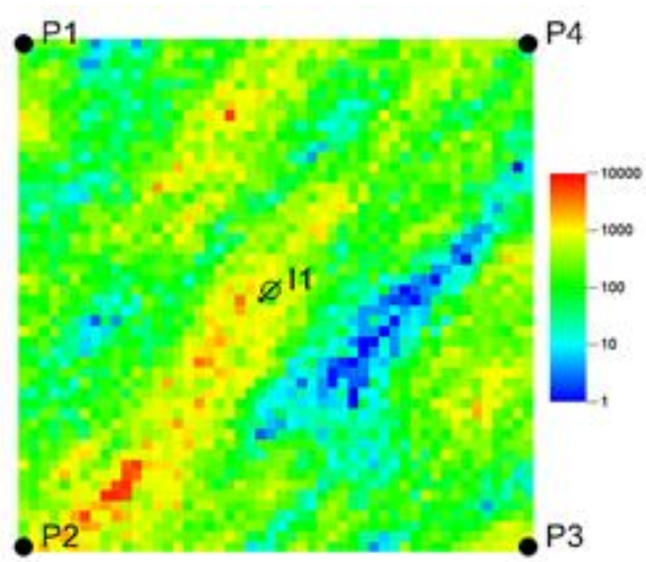

Fig. 2.4—2D heterogeneous example: Permeability distribution and well location.

The 2D example case (50x50 grid) has a fixed porosity of 0.23 and a spatially heterogeneous permeability **(Fig. 2.4).** We considered three base cases for injected polymer concentrations of 0 ppm, 500 ppm and 1000 ppm. The 0 ppm case corresponds to waterflooding. The field production and injection rate equals to 400 RB/D and the total production rate is equally divided among the producers in the base cases.

The high permeability channel (Fig. 2.4) connects the injector I1 to the producer P2 leading to preferential fluid movement towards P2 and reduced sweep efficiency during waterflooding. **Fig. 2.5** shows time-of-flight and water saturation maps after 2 years for the three base cases. The water front moves almost as a shock front with the addition of polymer resulting in delayed water breakthrough and increased water movement towards low permeability regions. However, even during polymerflooding, the front follows the preferential flow path towards producers in high permeability regions (Fig. 2.5). This gives opportunity for improving sweep efficiency during polymerflooding through rate control.

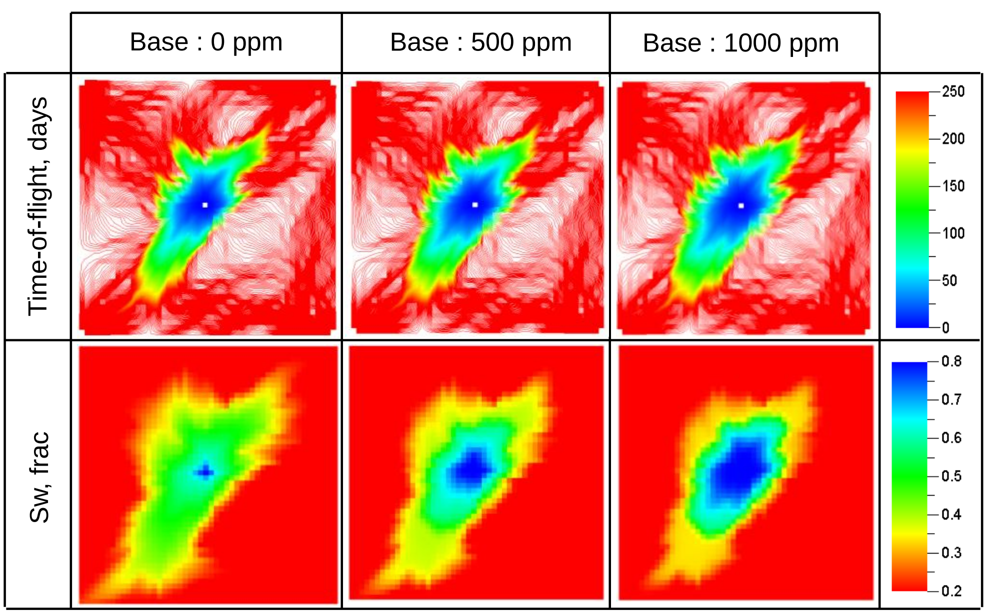

Fig. 2.5—Time-of-flight and water saturation maps after 2 years for the three base cases corresponding to 0 ppm, 500 ppm and 1000 ppm polymer concentration.

We carried out rate optimization for norm weights of 0 and 100 for the three base cases mentioned earlier, in timestep of 6 months for a total duration of 10 years. A norm weight of 0 corresponds to maximization of sweep efficiency while a norm weight of 100 results in accelerated production strategy. The constraints imposed during optimization are as follows:

- Field production rate ≤ 500 RB/D
- Well production rate ≤ 250 RB/D for each well
- Production FBHP ≥ 1000 Psia
- Injection FBHP ≤ 7000 Psia
- Water cut limit: 90%
- Max allowable polymer concentration at producers: 250 ppm

Fig. 2.6 shows the water saturation maps at three different times for the base cases corresponding to 0 ppm and 1000 ppm polymer concentration in the first and second column respectively. The respective saturation maps for sweep efficiency maximization (norm weight–0) are shown in the third and fourth column. It is evident from the last two columns that optimization results in a better sweep for both the cases by diverting flood front towards wells in low permeability regions.

The rate allocation for producer P2 for 1000 ppm polymerflooding is shown in **Fig. 2.7a.** As mentioned earlier, a high permeability channel connects producer P2 to injector I1.This results in water breakthrough after two years of production in the base case and the well shuts down after seven years of production owing to produced polymer concentration exceeding the maximum allowable limit of 250 ppm (Fig. 2.7b). During sweep efficiency maximization only (norm weight–0), a very low rate is allocated to producer P2 from the beginning to equalize the arrival time at all the producers by delaying water breakthrough at producer P2. Including production acceleration (norm weight–100) results in relatively higher rate allocation to producer P2 to achieve faster sweep leading to early water breakthrough.

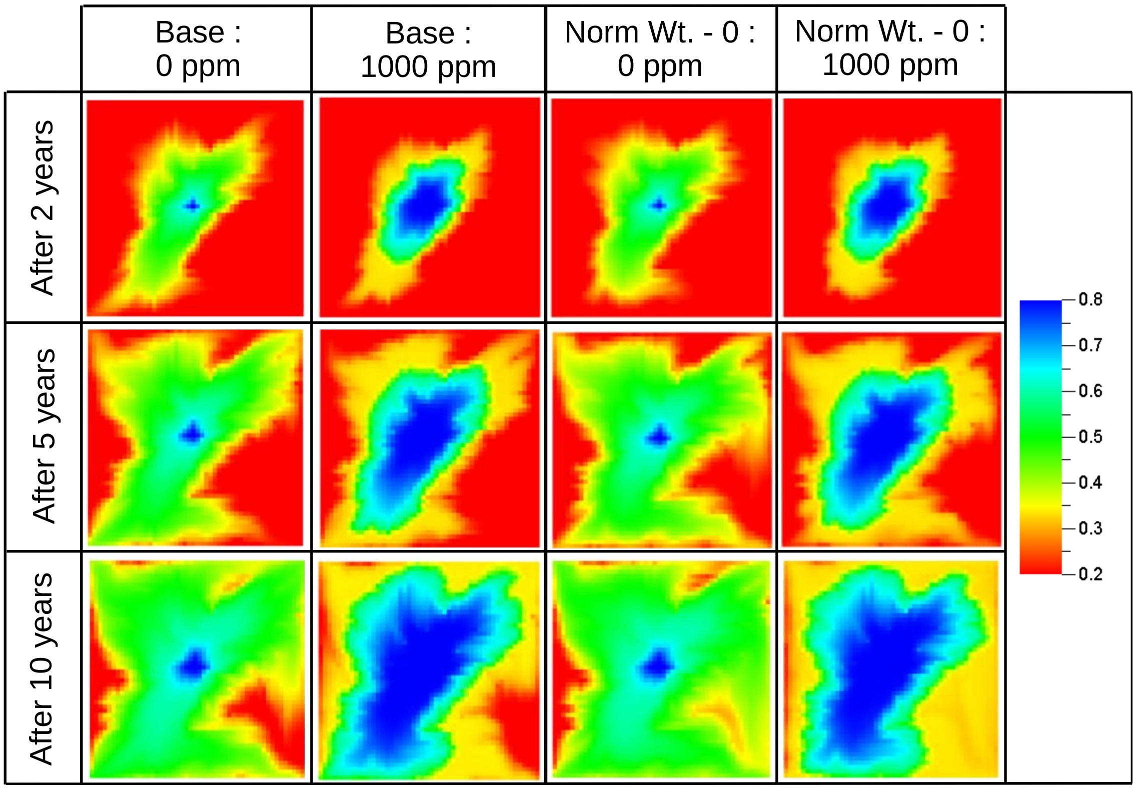

Fig. 2.6—Water saturation maps for base case and sweep efficiency maximization (norm weight–0) corresponding to 0 ppm and 1000 ppm polymer concentration at three different times.

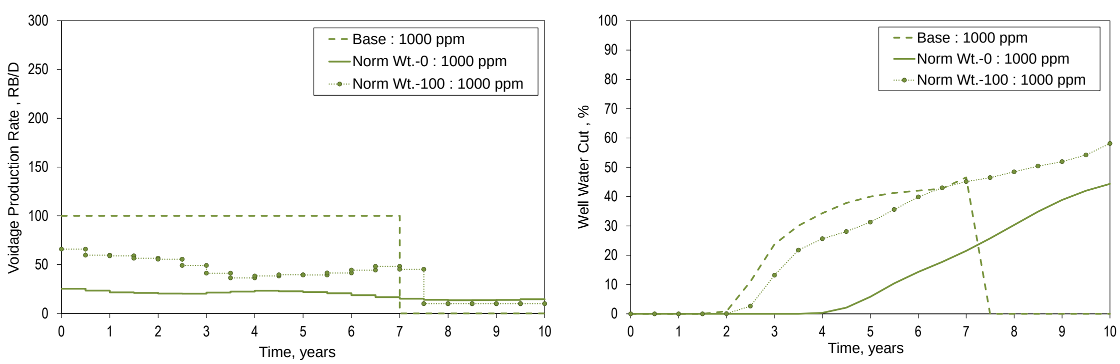

Fig. 2.7—(a) Production rates for well P2 for base case, sweep efficiency maximization (norm weight–0) and production acceleration (norm weight–100) at 1000 ppm polymer concentration (b) Water cut for well P2 for respective cases.

The rate allocation for producer P3 for 1000 ppm polymerflooding is shown in **Fig. 2.8a.** Because of presence of a barrier, the well has least connectivity to the injector. Water breakthrough occurs in producer P3 after six years of production in the base case as opposed to two years for producer P2 (Fig. 2.8b). During sweep efficiency maximization (norm weight–0), a very high rate is allocated to producer P3 from the beginning to equalize the arrival time at all the producers. Production acceleration (norm weight–100) results in relatively higher rate allocation to producer P3 to achieve faster sweep leading to early water breakthrough.

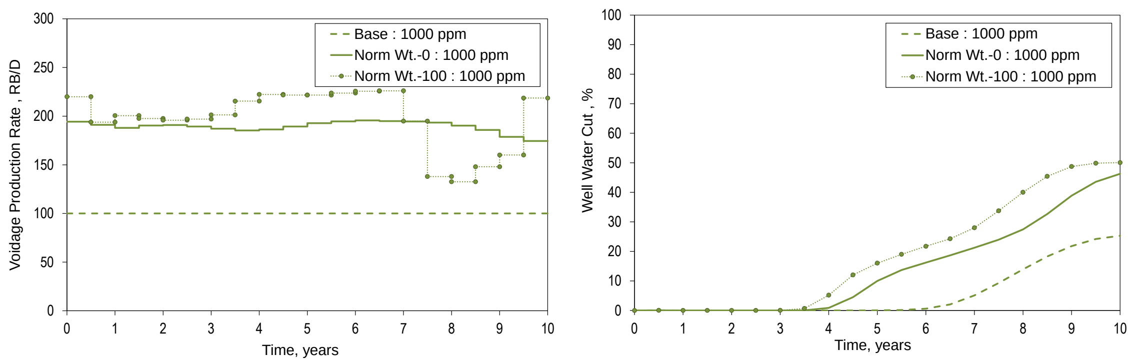

Fig. 2.8—(a) Production rates for well P3 for base case, sweep efficiency maximization (norm weight–0) and production acceleration (norm weight–100) at 1000 ppm polymer concentration (b) Water cut for well P3 for respective cases.

The effect of rate optimization on field water cut is in accordance to the well performances discussed earlier. The optimal rates corresponding to sweep efficiency maximization (norm weight–0) result in delayed water breakthrough and reduced water recycling **(Fig. 2.9a).** However, the injection and production rates increase during acceleration (norm weight–100), resulting in early water breakthrough (Fig. 2.9b). **Fig. 2.10a** shows the increase in oil recovery for the base case with increase in polymer concentration. Maximizing sweep efficiency (norm weight–0) results in further increase in oil recovery for the three cases for approximately the same amount of water injection

(Fig. 2.10b). Production acceleration (norm weight–100) results in further increase in oil recovery owing to increased cumulative water injection.

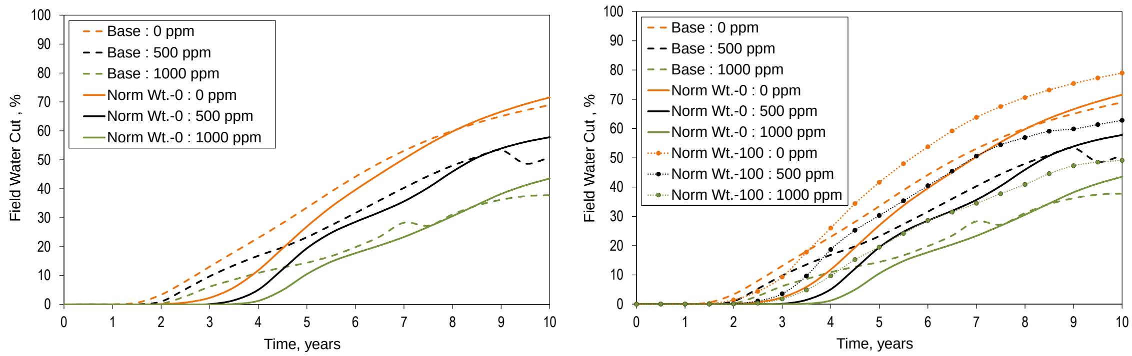

Fig. 2.9—(a) Field water cut for base case and sweep efficiency maximization (norm weight–0) corresponding to 0 ppm, 500 ppm and 1000 ppm polymer concentration (b) Effect of production acceleration (norm weight–100) on field water cut corresponding to 0 ppm, 500 ppm and 1000 ppm polymer concentration.

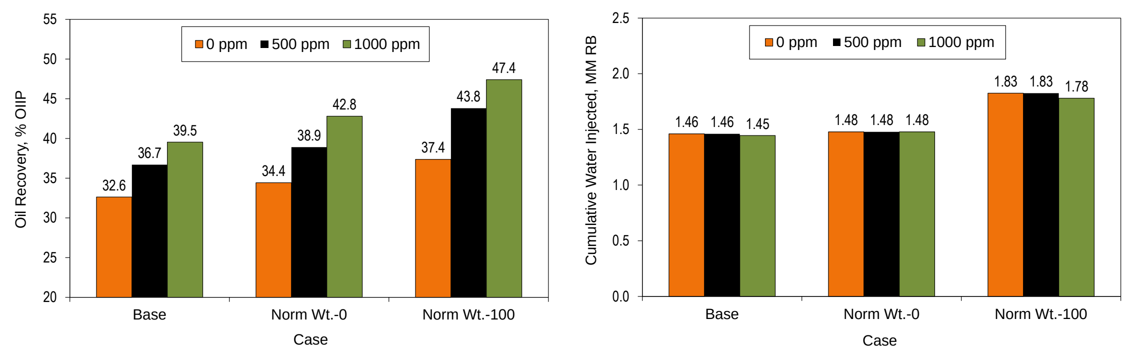

Fig. 2.10—(a) Oil recovery (w.r.t OOIP) after 10 years for base case, sweep efficiency maximization (norm weight–0) and production acceleration (norm weight–100) corresponding to 0 ppm, 500 ppm and 1000 ppm polymer concentration (b) Cumulative water injection for respective cases.

It is interesting to express the above results in terms of field-wide utility factor which is defined as the amount of polymer required per incremental oil volume produced (Clemens et al. 2010). Utility factor gives an indication of incremental operating cost and serves as a key parameter to assess the viability of polymer injection project. **Fig.**

2.11 shows the utility factor for 500 ppm and 1000 ppm polymerflood for various cases. Maximizing sweep efficiency (norm weight–0) results in decrease in utility factor for both 500 ppm and 1000 ppm polymerflood. Production acceleration (norm weight–100) further decreases the utility factor owing to increased cumulative water injection. These results clearly demonstrate the practical viability of our approach.

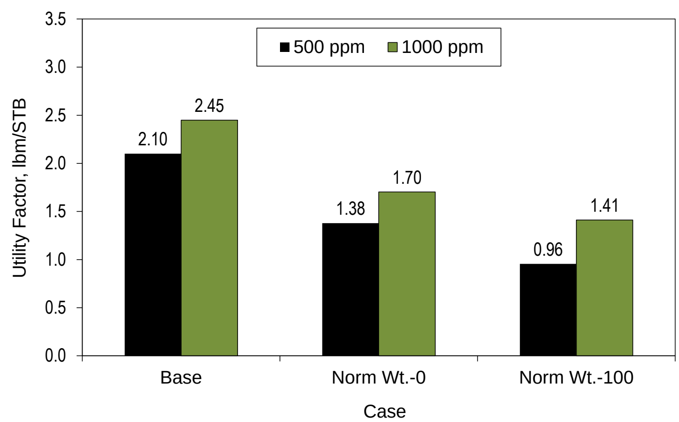

Fig. 2.11—Utility factor for base case, sweep efficiency maximization (norm weight–0) and production acceleration (norm weight–100) corresponding to 500 ppm and 1000 ppm polymer concentration.

2.4 Synthetic Field Example

In this section we illustrate the practical feasibility of the rate optimization approach for polymerflooding using a field-scale example.

The injection and production data used in this example correspond to the Goldsmith field (Jasek et al. 1998) which is located on eastern flank of the Central Basin Platform in the Permian basin. Two structural closures, 'north dome' and 'south dome', exist on the San Andres unit with the productive interval lying at an approximate depth of 4200 ft. The Goldsmith San Andres Unit (GSAU) consists of the south flank of the north dome and the entire south dome **(Fig. 2.12).** Waterflooding began in GSAU in 1954 with peripheral injection below the producing oil-water contact. By 1995, majority of wells were plugged due to high water cut, when it was planned to carry out a pilot study for CO_2 miscible flooding. To our knowledge, no polymerflooding was carried out in this field. Nevertheless, the highly heterogeneous permeability distribution makes it a good candidate for illustrating our approach. We adjusted reservoir properties, specifically permeability, to allow for polymer injection.

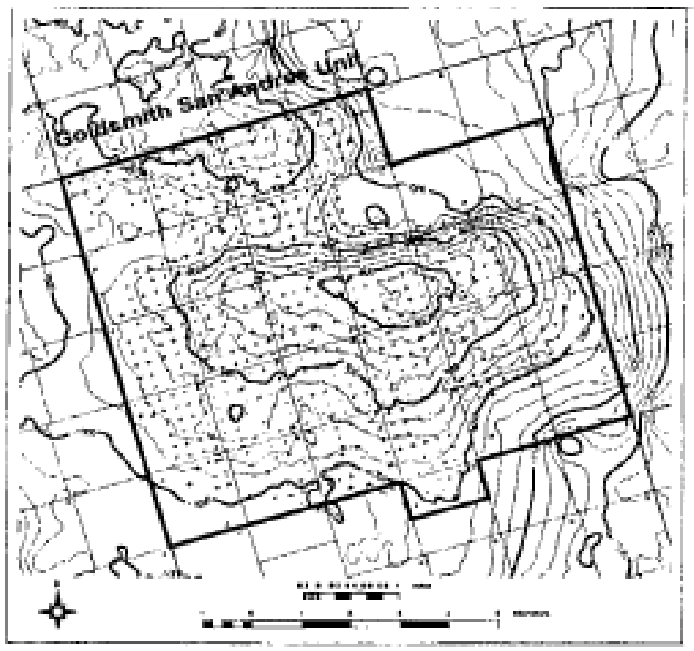

Fig. 2.12—GSAU top of San Andres formation structure map (Jasek et al. 1998).

We applied our proposed approach to the CO_2 pilot area in the GSAU, which consists of nine inverted five-spot patterns covering 320 acres. The study area was discretized into 58x53x10 mesh containing 11 water injectors and 31 producers. The base case considers the actual field production/injection history during the first 21 years of waterflooding **(Fig. 2.13).** Seven time-steps were considered to account for changing production/injection rates and well schedule.

A 500 ppm polymerflood for the base case results in incremental oil recovery of 4.7% OOIP over the waterflood. We demonstrate that the rate optimization approach suggest a production strategy resulting in better sweep during polymerflooding. Both production and injection rates were optimized, while polymer injection concentration was kept constant at 500 ppm. The production wells were subdivided into groups based on sensitivity S_{ij} which quantifies the changes in arrival time at producer i because of small changes in the rate of injector j. The group selection is dynamic and repeated for every time-step to account for changing production/injection rates, mobility effects and infill drilling.

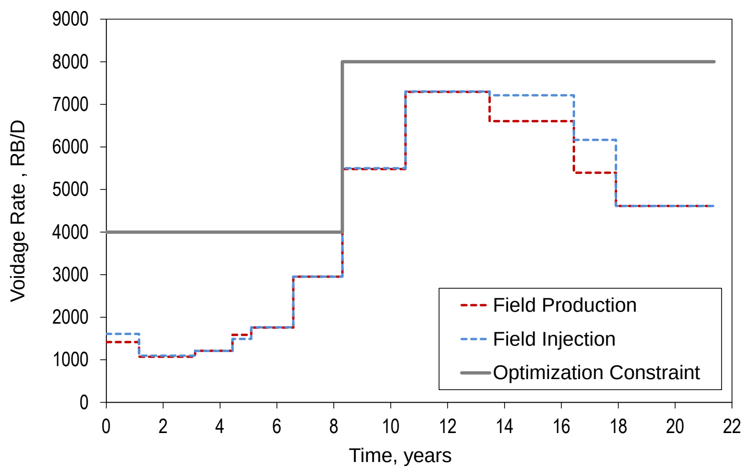

Fig. 2.13—Field production/injection history. Maximum production/injection rate: 4000 RB/D (first 8 years), 8000 RB/D (next 13 years).

We obtained the optimal rates for maximizing sweep efficiency (norm weight–0) for 0 ppm and 500 ppm polymerflood. The 0 ppm polymerflood corresponds to waterflood. Additionally, an accelerated production strategy was obtained using a norm weight of 10000. The constraints imposed during optimization are as follows:

- Field production rate ≤ 4000 RB/D (first 8 years), 8000 RB/D (next 13 years)
- Well production rate ≤ 900 RB/D for each well
- Well injection rate ≤ 1200 RB/D for each well
- Production FBHP ≥ 1000 Psia

• Injection FBHP ≤ 4500 Psia

• Water cut limit: 98%

• Max allowable polymer concentration at producers: 450 ppm

2.4.1 Polymerflood Optimization Using Single Geologic Model

In this section, we discuss application of our approach for a single realization **(Fig. 2.14).** The impact of geological uncertainty is not considered during this optimization and will be discussed in the next example.

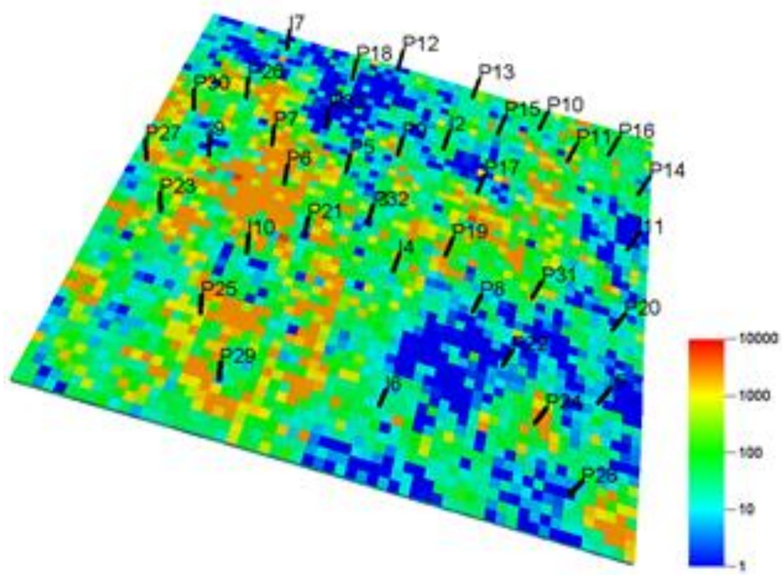

Fig. 2.14—Field permeability distribution and well location.

Maximizing sweep efficiency (norm weight–0) result in delayed water breakthrough and reduced water recycling for both the base cases of 0 ppm and 500 ppm **(Fig. 2.15a).** During production acceleration (norm weight–10000), the injection and production rates increases resulting in early water breakthrough as expected (Fig. 2.15b). **Fig. 2.16a** shows the increase in oil recovery for the base case with polymer injection. The optimal rates corresponding to norm weight of 0 and 10000 result in further increase in oil recovery for the two cases. It should be noted that cumulative water injected during sweep efficiency maximization is approximately same as that for the base case (Fig. 2.16b). The decrease in utility factor for sweep efficiency maximization (norm weight–0) during polymerflood **(Fig. 2.17)** demonstrates the practical feasibility of our approach. Production acceleration results in further decrease in the utility factor owing to increased cumulative water injection.

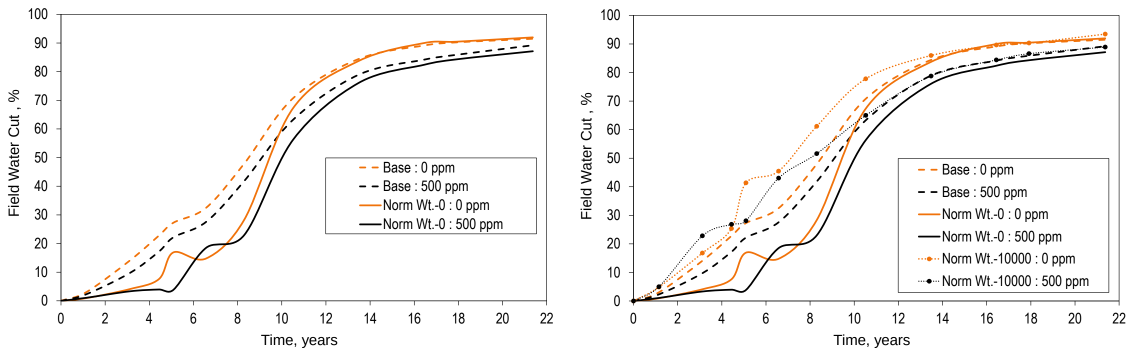

Fig. 2.15—(a) Field water cut for base case and sweep efficiency maximization (norm weight–0) corresponding to 0 ppm and 500 ppm polymer concentration (b) Effect of production acceleration (norm weight–10000) on field water cut corresponding to 0 ppm and 500 ppm polymer concentration.

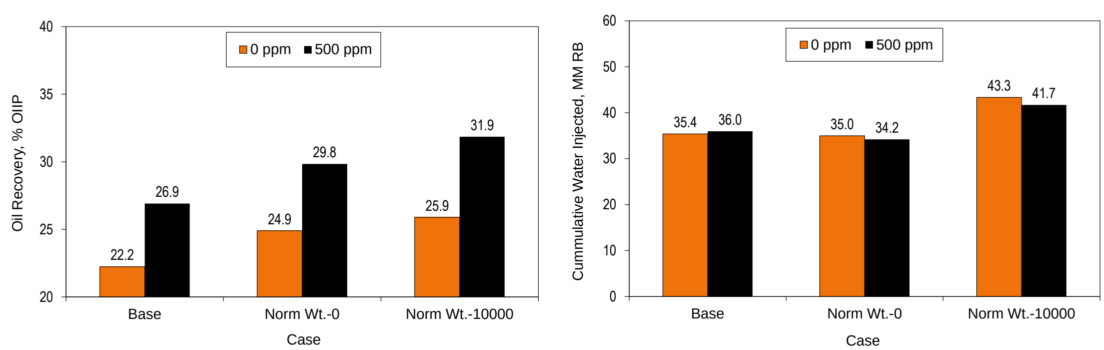

Fig. 2.16—(a) Oil recovery (w.r.t OOIP) after 21 years for base case, sweep efficiency maximization (norm weight–0) and production acceleration (norm weight–10000) corresponding to 0 ppm and 500 ppm polymer concentration (b) Cumulative water injection for respective cases.

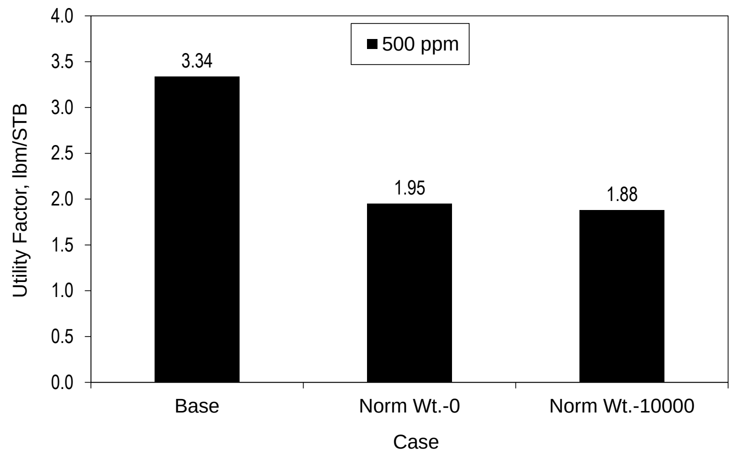

Fig. 2.17—Utility factor after 21 years for base case, sweep efficiency maximization (norm weight–0) and production acceleration (norm weight–10000) corresponding to 500 ppm polymer concentration.

2.4.2 Polymerflood Optimization Using Multiple Geologic Models

In this section we discuss application of our approach using multiple realizations to address geological uncertainty. Multiple distributions of porosity were generated using Sequential Gaussian Simulation, conditioned to well data and secondary seismic attributes. The permeability distributions were generated via cloud transform based on porosity-permeability relationship.

The realization from the previous case was considered as the reference realization. We carried out optimization using 10 realizations (including reference realization) using the expected value formulation as discussed before, under risk neutral conditions (*r*–0). To illustrate the variability amongst the geologic realizations, we have shown the permeability distribution in the top layer for each of the 10 realizations in **Fig. 2.18.** The optimized rates thus obtained were applied to a blind realization which was not included in the optimization process. To illustrate the robustness of our approach, we applied to the same blind realization the optimal rates obtained from the single realization optimization as discussed in the previous section. For comparison purposes, the top layer permeability for the blind realization used to test the optimization methods is shown in **Fig. 2.19.**

Fig. 2.20 compares the performance of the blind realization in terms of field water cut and oil recovery under two scenarios. The first scenario uses the rate derived from optimization of single realization (SR), whereas the second scenario accounts for geologic uncertainty based on the expected value of arrival time residuals from multiple realizations (MR). We used norm weight of 0 for both the scenarios. The optimal rates corresponding to MR optimization resulted in higher oil recovery and lower utility factor **(Fig. 2.21)** over SR optimization, when applied to the blind realization. Since, the realizations have been generated using a single variogram (including blind realization), MR optimization doesn't result in significant reduction in utility factor over SR optimization.

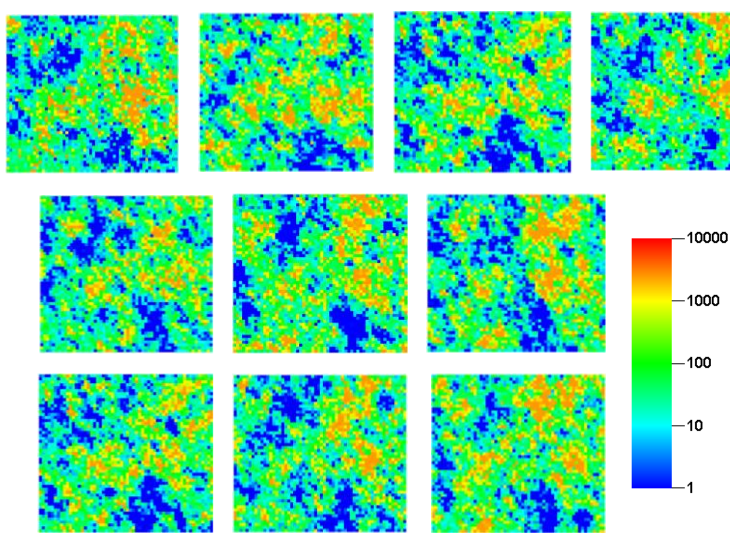

Fig. 2.18—Permeability (layer 1) for 10 realizations used in stochastic optimization.

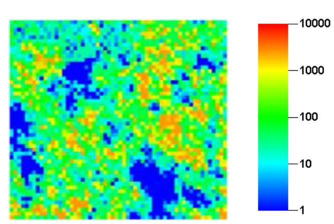

Fig. 2.19—Permeability (layer 1) for blind realization.

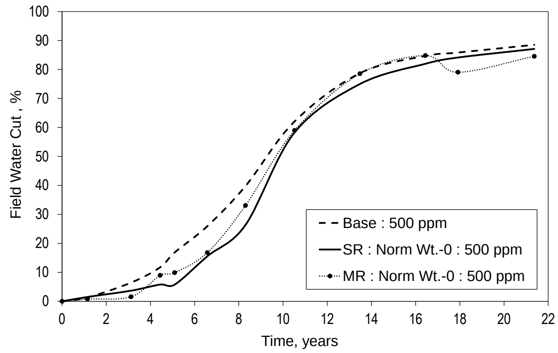

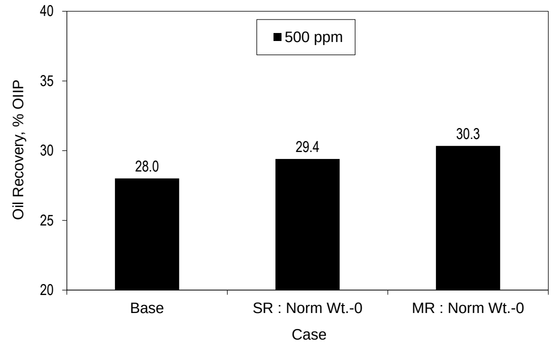

Fig. 2.20—(a) Field water cut for base case and sweep efficiency maximization (norm weight–0) corresponding to 500 ppm polymer concentration for single realization (SR) and multiple realizations (MR) (b) Oil recovery (w.r.t OOIP) after 21 years for respective cases.

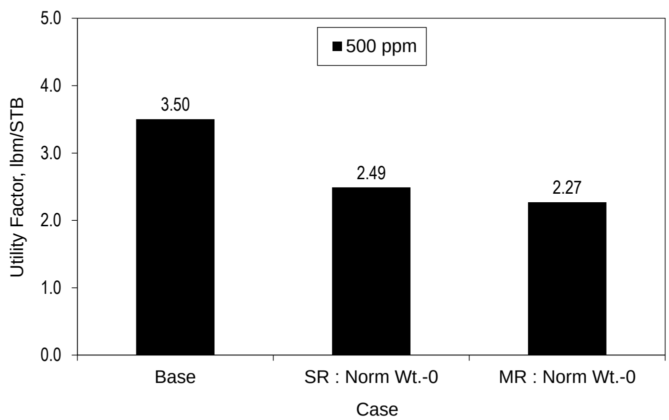

Fig. 2.21—Utility factor after 21 years for base case and sweep efficiency maximization (norm weight–0) corresponding to 500 ppm polymer concentration for single realization (SR) and multiple realizations (MR).

Finally, in **Fig. 2.22** we show the oil saturation after 21 years for base case and reduction in oil saturation with sweep efficiency maximization (norm weight–0) corresponding to 500 ppm polymer concentration for rates derived from single realization and multiple realizations optimization. This clearly demonstrates the robustness of the approach to account for geologic uncertainty and is consistent with the improvement in oil recovery.

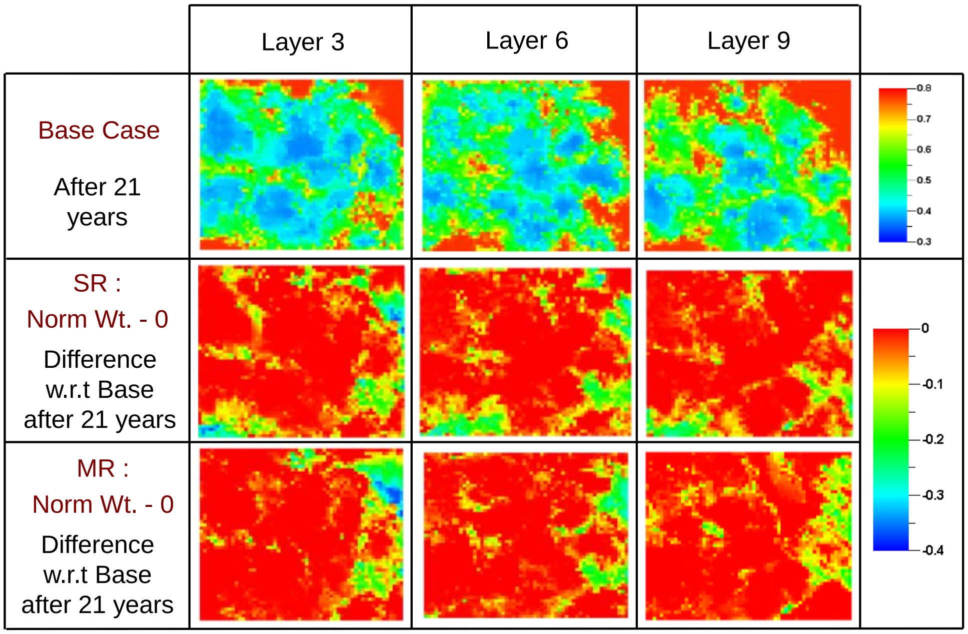

Fig. 2.22—Oil saturation after 21 years for base case and reduction in oil saturation with sweep efficiency maximization (norm weight–0) corresponding to 500 ppm polymer concentration for single realization (SR) and multiple realizations (MR).

2.5 Summary

In this chapter, we demonstrated an efficient approach for optimizing polymerflood via rate control. The approach relies on making an optimal decision based on a compromise between maximizing sweep efficiency and accelerating production. Because of analytical computation of the sensitivities and the gradient and Hessian of the objective function, the approach is computationally efficient and suitable for large field cases. The hierarchy of rate and pressure constraints is captured during optimization through comprehensive constraint matrices. Moreover, the approach can account for geologic uncertainty using multiple realizations via a stochastic optimization framework.

We show that the approach yields robust rates using a 3D field-scale example. Significant improvement in oil recovery and reduction in polymer recycling was achieved over the base case with the application of rate optimization. Geologic uncertainty was addressed using 10 history matched realizations for optimization and applying the rates derived from optimization to a blind realization.

CHAPTER III

OPTIMAL CO_2 FLOOD MANAGEMENT VIA RATE CONTROL

Carbon dioxide has been successfully used as EOR agent for decades because of its favorable properties of swelling oil, reducing oil viscosity and reducing residual oil saturation (Holm and Josendal 1974; Stalkup 1983). However, despite its high local displacement efficiency, the process has poor sweep efficiency due to viscous fingering caused by unfavorable mobility ratio and gravity segregation caused by density difference between injected and displaced phases (Christie and Bond 1987). Caudle and Dyes (1958) proposed the control of this fingering and poor conformance by injecting water along with gas to reduce gas mobility. Strategies like water-alternating-gas (WAG) injection have been thus applied in field to mitigate this problem.

The sweep efficiency during gasflood depends upon mobility ratio (Habermann 1960), viscous-to-gravity ratio (Craig et al. 1957; Spivak 1974) and reservoir heterogeneity (Koval 1963; Fayers et al. 1992). The design parameters influencing the sweep efficiency during CO_2 flood have been discussed by several authors (Green and Willhite 1998; Jarrell et al. 2002). Moreover, modification to uniform coinjection of water and gas (Stone 1982; Jenkins 1984) have been suggested by Rossen et al. (2010) to maximize the distance to the point of segregation of injected gas/water mixture. However, guidelines for selection of optimal well production/injection rates during CO_2 flood still remain to be established.

In this chapter, we extend the role of rate optimization for CO_2 flooding to maximize sweep efficiency and minimize CO_2 recycling by delaying CO_2 breakthrough. First, we outline the details of CO_2 flood modeling considered for our work. Then, we discuss the modification made to the approach (Taware et al. 2010). Finally, we demonstrate the robustness and application of our approach using a 2D heterogeneous cross section and a synthetic field application for CO_2 flood and WAG.

3.1 CO_2 Flood Modeling

Depending upon the properties of the fluids at reservoir condition, the displacement of the oil by CO_2 can be classified as immiscible and miscible (Holm and Josendal 1974). The immiscible displacement occurs at pressures below minimum miscibility pressure (MMP) during which incremental oil is recovered because of oil swelling, reduced oil viscosity and lower interfacial tension between CO_2 and oil. However, the interfacial tension is not zero resulting in some residual oil saturation. On the other hand, miscible displacement occurs at pressures above MMP, in which over 95% of oil contacted can be displaced because of zero interfacial tension, in addition to factors mentioned earlier.

We used a three-component modified black oil model (ECLIPSE©) consisting of reservoir oil, injection gas (solvent) and water to describe miscible displacement of oil by CO_2 as suggested by Todd and Longstaff (1972). The Todd-Longstaff empirical model account for physical dispersion by using mixing parameter ω, the value of which lies between 0 and 1, to represent the size of the dispersed zone in each grid cell. The solvent and reservoir oil components are assumed to be miscible in all proportions and consequently only one hydrocarbon phase exists in the reservoir. The model then computes effective viscosity and density for oil-solvent system based on ω.

We considered ω = 0.67 for our studies with a corresponding residual oil saturation of 12%. Field pressure during CO_2 flood was maintained above MMP for all cases studied to maintain miscibility.

3.2 CO_2 Flood Rate Optimization

The streamline-based rate optimization approach discussed earlier is used to obtain an optimal as well as accelerated production strategy for CO_2 flooding. We trace streamlines using the fluid fluxes derived from the finite-difference flow simulation (Jimenez et al. 2008). Our approach relies on equalizing arrival time of the flood front at all producers to maximize the areal sweep efficiency and an additional 'norm' constraint on the arrival times to achieve high viscous-to-gravity ratio (VGR) to minimize gravity segregation. VGR as defined by Fayers and Muggeridge (1990) and written by Tchelepi and Orr (1994) for a cross section of thickness *h* and length *L* is:

$$VGR = 2\left(\frac{\bar{v}\Delta\mu}{\Delta\rho g k_v}\right)\left(\frac{h}{L}\right) \quad (3.1)$$

where $\bar{v}$ is the average Darcy velocity, $\Delta\mu$ is viscosity difference between oil and CO_2, $\Delta\rho$ is density difference between oil and CO_2 and k_v is the geometric mean of permeability. The 'optimal' rate strategy is decided based upon a compromise between maximizing sweep efficiency and production acceleration. The geologic uncertainty is accounted using a stochastic framework for multiple realizations.

3.2.1 Optimization After CO_2 Breakthrough

Since we have formulated our optimization in terms of arrival time of the CO_2 front at the producers, a natural question arises that what happens after CO_2 breakthrough. The optimization is carried out after CO_2 breakthrough at a well by incorporating the well gas-oil ratio (GOR) into the objective function as follows:

$$t'_{i,m}(\mathbf{q}) = t_{i,m}(\mathbf{q}) * \left(1 - f_{gas\,i,m}\right)^{\alpha} \quad (3.2)$$

where

$$f_{gas\ i,m} = \frac{\text{Well GOR}}{\text{Max allowable well GOR}} \quad (3.3)$$

In the above expression, the arrival time, $t_{i,m}$, at well *i* belonging to group *m* has been altered to incorporate the well GOR, $f_{GOR\ i,m}$. The modified arrival time is the same as the original arrival time if GOR is zero. When the well GOR is greater than zero, the original arrival time will be rescaled based on the GOR level w.r.t the maximum allowable limit. The extent of reduction can be controlled by the exponent term, α. As a consequence, the rate allocation to the well will be lowered in relation to the wells with less GOR. The well is shut when the GOR reaches the maximum limit.

3.3 Illustration of the Approach

In this section, we illustrate our approach for CO_2 flooding using a 2D heterogeneous cross section **(Fig. 3.1).** The cross section (200x1x180 grid) has a fixed porosity of 0.10 and spatially heterogeneous permeability. A producer and an injector with 45 ICVs each have been completed on either sides of the cross section. Following constraints were imposed during rate optimization:

- Well production/injection rate $\leq$ 9000 RB/D
- ICV production/injection rate $\leq$ 450 RB/D
- Production FBHP $\geq$ 2000 psia
- Injection FBHP $\leq$ 6000 psia
- ICV GOR limit: 100 Mscf/STB

The base case considers reactive control where production/injection ICV rate equals to 150 RB/D. The production ICVs are shut when their GOR exceeds 100 Mscf/STB. The combined effects of heterogeneity, viscous fingering and gravity segregation lead to preferential CO_2 movement towards the top production ICVs in the base case **(Fig. 3.2a).** This results in early CO_2 breakthrough and reduced sweep efficiency. Fig. 3.2b shows the time-of-flight map after 2 years for the base case, which suggest that there is sufficient scope for improving sweep and delaying CO_2 breakthrough by equalizing CO_2 front arrival time at production ICVs through rate control.

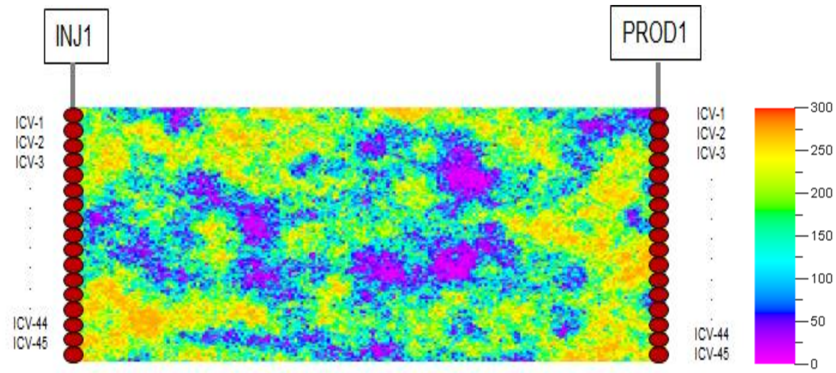

Fig. 3.1—2D cross section: Permeability distribution and well location.

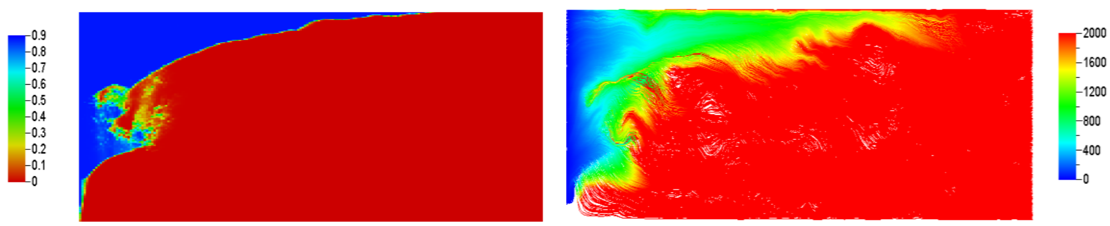

Fig. 3.2—(a) Gas saturation after 2 years of CO_2 injection for the base case. (b) Corresponding time-of-flight map in days for the base case.

We obtained optimal rates for norm weights of 0, 10, 100 and 1000 for 20 years in timestep of 6 month for the base case mentioned above. A norm weight of 0 corresponds to maximizing sweep efficiency while norm weights of 10, 100 and 1000 result in accelerated production strategy.

Fig. 3.3 shows the gas saturation maps at four different times for base case, sweep efficiency maximization (norm weight–0) and acceleration (norm weight–1000). The sweep is dominated by gravity segregation for base case. For norm weight of 0, the displacement rate is sufficiently low so that the gravity tongue still exists. However, optimal rates corresponding to norm weight of 0 results in improved injection efficiency, as explained later. The transition zone between oil and gas is relatively thin compared to reservoir thickness as mentioned by Fayers and Muggeridge (1990). It has been shown in Fig. 2.6 that equalizing front arrival time maximizes areal sweep for waterflood and polymerflood. However, we don't see those effects for this case which is being limited to a cross-section. As the norm weight increases, the production rates and CO_2 injection rates approach the upper limit for ICVs and well. This increases VGR as shown in **Fig. 3.4** and, the gravity tongue loses strength and becomes smaller. The VGR has been obtained by using geometric mean of permeability for the heterogeneous cross section. Because of low displacement rate, optimization corresponding to norm weight of 0 results in low VGR.

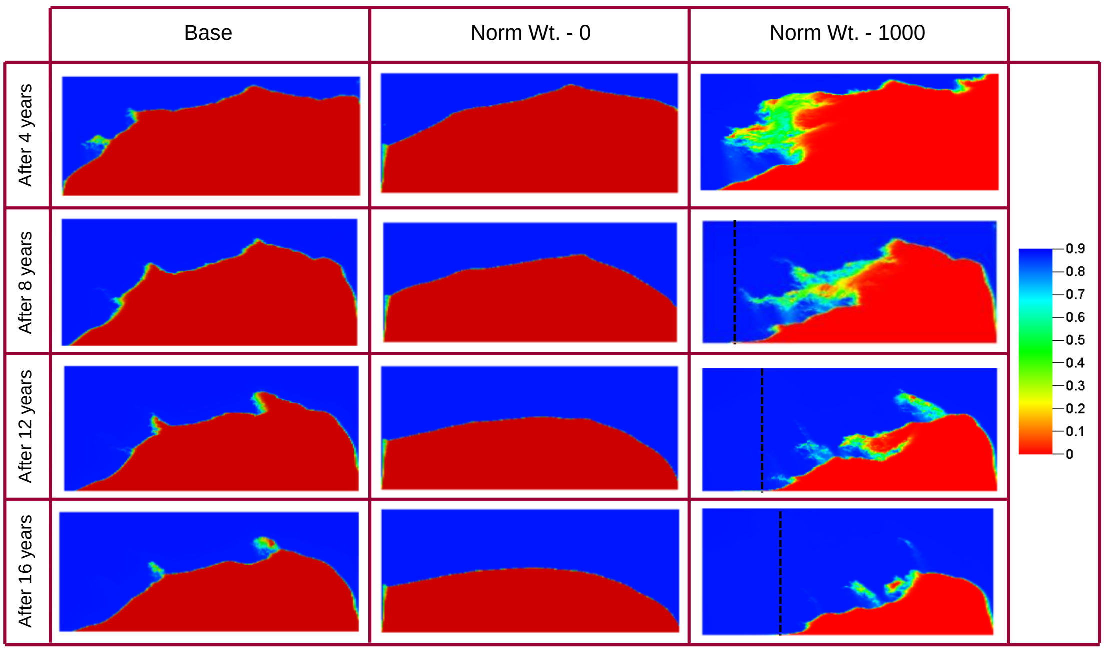

Fig. 3.3—Gas saturation maps for base case, sweep efficiency maximization (norm weight–0) and production acceleration (norm weight–1000) at four different times.

The cumulative voidage production for ICV-1 of producer is shown in **Fig. 3.5a** for base case, sweep efficiency maximization (norm weight–0) and acceleration (norm weight–1000). ICV-1 gets shut when its GOR exceeds 100 Mscf/STB during base case and sweep efficiency maximization. Increasing the norm weight reduces gravity segregation, thus allowing ICV-1 to produce for a longer duration without CO_2

breakthrough. Fig. 3.5b shows cumulative voidage production for ICV-45 of producer for respective cases. In order to divert CO_2 towards lower ICVs, their production rate approaches the maximum limit for norm weight of 0. This results in high cumulative production for sweep efficiency maximization as compared to base case. However, increasing norm weight reduces gravity segregation and lower rates are allocated to producer's lower ICVs.

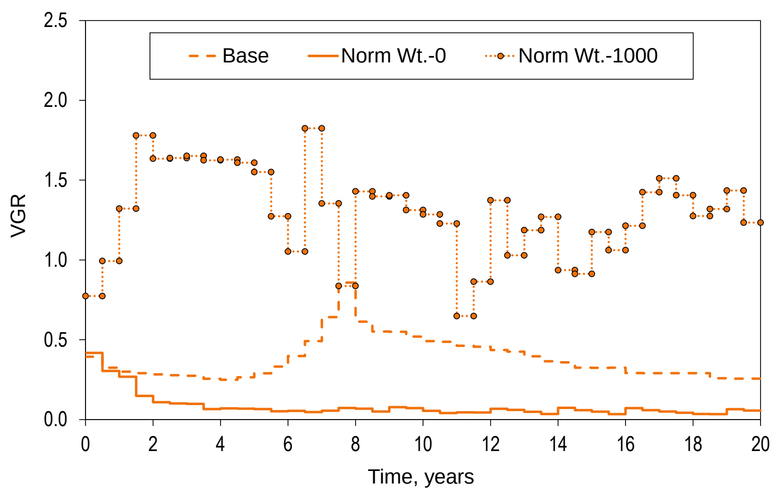

Fig. 3.4—VGR for base case, sweep efficiency maximization (norm weight–0) and production acceleration (norm weight–1000) at different times.

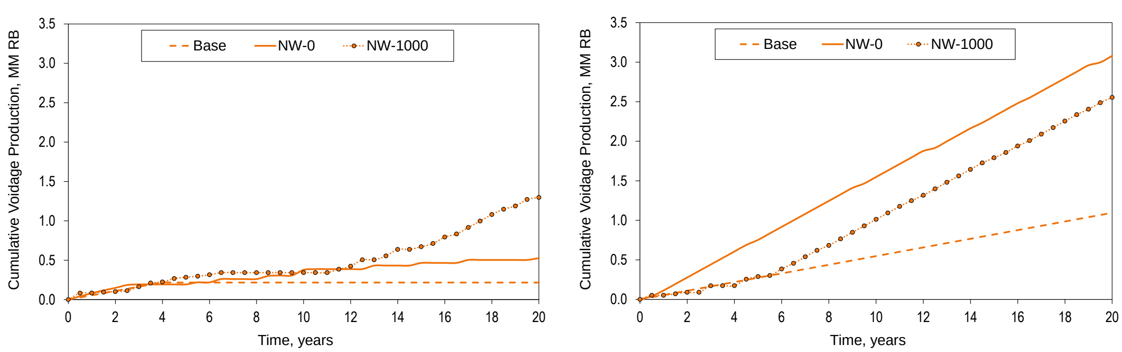

Fig. 3.5—(a) Cumulative voidage production for ICV-1 (PROD1) for base case, sweep efficiency maximization (norm weight–0) and production acceleration (norm weight–1000). (b) Cumulative voidage production for ICV-45 (PROD1) for respective cases.

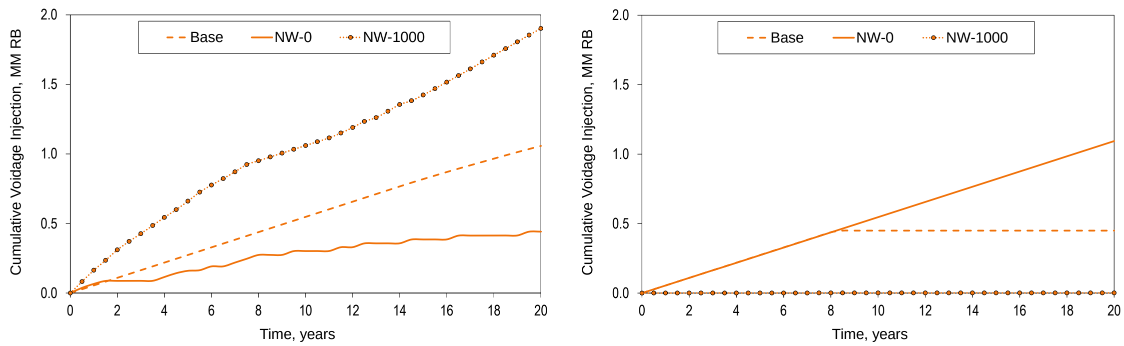

Fig. 3.6—(a) Cumulative voidage injection for ICV-1 (INJ1) for base case, sweep efficiency maximization (norm weight–0) and production acceleration (norm weight–1000). (b) Cumulative voidage injection for ICV-45 (INJ1) for respective cases.

Fig. 3.6a shows that the cumulative voidage injection for ICV-1 of injector for sweep efficiency maximization (norm weight–0) is less than that for base case. The cumulative voidage injection for ICV-45 of injector for respective cases is shown in Fig. 3.6b. ICV-45 gets shut when its injection FBHP exceeds 6000 psia during base case and acceleration. In order to divert CO_2 towards lower ICVs, the injection rate from lower ICVs approaches the maximum limit for maximizing sweep efficiency.

The effect of rate optimization on field GOR is in accordance to the ICV performance discussed earlier. The optimal rates corresponding to sweep efficiency maximization (norm weight–0) result in delayed CO_2 breakthrough **(Fig. 3.7a).** However, the injection and production rates increase during acceleration (norm weight–1000), resulting in early CO_2 breakthrough and more CO_2 recycling (Fig. 3.7b).

The increase in oil recovery with maximizing sweep efficiency (norm weight–0) is shown in **Fig. 3.8a.** It should be noted that cumulative CO_2 injected for maximizing sweep efficiency is significantly less compared to that for base case (Fig. 3.8b). Acceleration (norm weight–10, 100 and 1000) results in increase in oil recovery owing to improved VGR caused by higher CO_2 injection rates.

It is interesting to express the results for rate optimization in terms of field-wide injection efficiency which is defined as ratio of cumulative oil produced to cumulative CO_2 injected at reservoir conditions (Datta-Gupta and King 2007). Injection efficiency thus indicates how efficiently injected CO_2 is used, a lower value of which corresponds to large CO_2 recycling. **Fig. 3.9** illustrates the injection efficiency for various norm weights. The optimal rates corresponding to norm weight of 0 increase injection efficiency significantly over base case. The results clearly demonstrate the trade-off between improving recovery by accelerating production and improving injection efficiency by reducing CO_2 recycling.

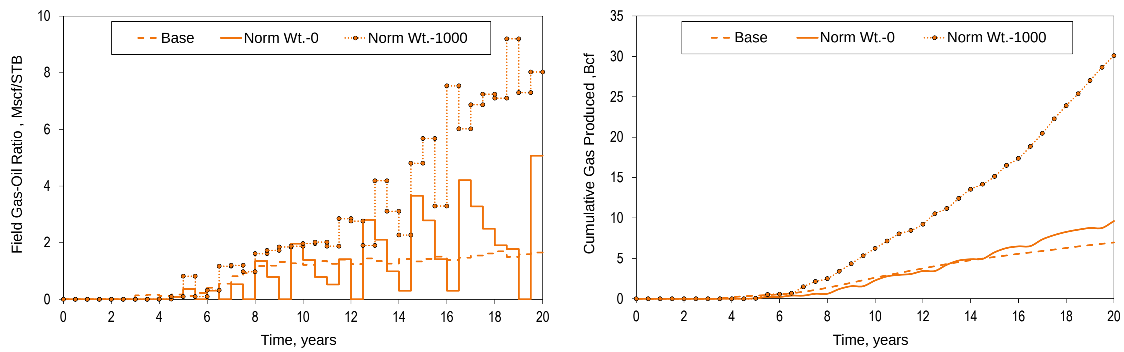

Fig. 3.7—(a) Field GOR for base case, sweep efficiency maximization (norm weight–0) and production acceleration (norm weight–1000). (b) Cumulative field gas production for respective cases.

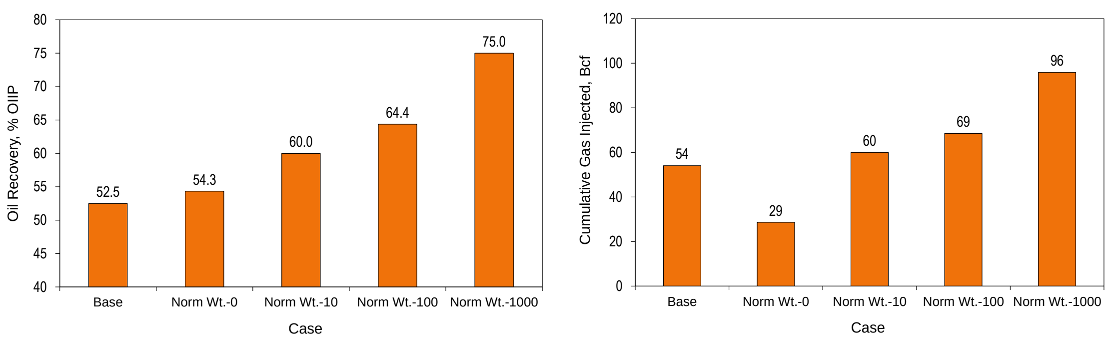

Fig. 3.8—(a) Oil recovery (w.r.t OOIP) after 20 years of CO_2 flood for base case, sweep efficiency maximization (norm weight–0) and production acceleration (norm weight–10, 100 and 1000). (b) Cumulative gas injection for respective cases.

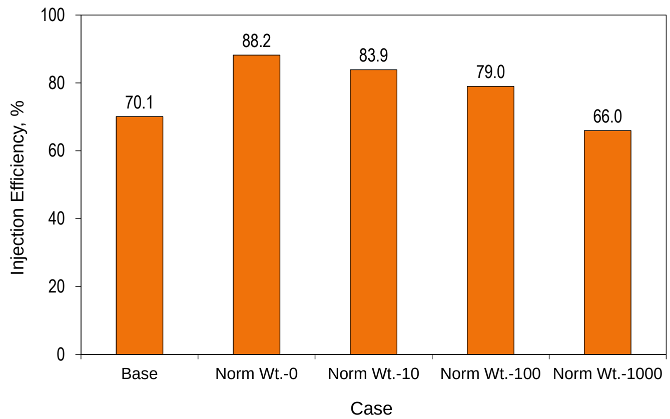

Fig. 3.9—Injection efficiency for base case, sweep efficiency maximization (norm weight–0) and production acceleration (norm weight–10, 100 and 1000).

3.4 Synthetic Field Example

In this section, we illustrate the application of the rate optimization approach for CO_2 and WAG flooding using a 3D synthetic field case, the Brugge field. This field case was set up as part of an SPE Applied Technology Workshop (ATW) to test the use of history matching and flood optimization methods (Peters et al. 2010).

The structure of the Brugge field consists of an E-W elongated half-dome with a large boundary fault at its north edge, and one internal fault with a modest throw at an angle of around 20 degrees to the north boundary fault. The field properties are based on a North Sea Brent-type field. A set of 104 realizations were generated based on the reservoir properties and well log attributes extracted from a high-resolution geologic model. The simulation model consists of 60000 grid cells with 9 layers. It has 20 vertical producers completed mainly in the top 8 layers and 10 peripheral injectors completed in all 9 layers **(Fig. 3.10).**

The first 10 years of the production history of the field was provided for history matching purposes (Peters et al. 2010). The production history was based on a ‘true model’ response with added noise. The closed loop control approach consisted of two steps: (i) Model updating using the field production history for the first 10 years and (ii) Production optimization over the next 20 years. In this study, we focus on the rate optimization part for the Brugge field. The details of the history matching have been discussed in a previous paper (Alhuthali et al. 2010). We carry out the optimization for 20 years under following three scenarios:

- Rate optimization for CO_2 flooding using a single history matched model (reference realization).
- Rate optimization for CO_2 flooding using 10 history matched models (including reference realization) and application of the optimized rates on a blind realization.
- Rate optimization for WAG flooding using reference realization.

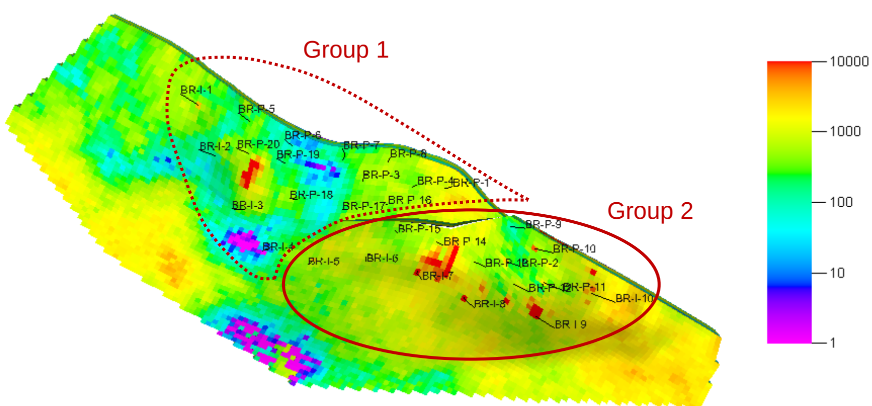

Fig. 3.10—Brugge field: Permeability distribution and well location.

The wells were divided into two groups based on the location of the internal fault (Fig. 3.10) to calculate analytical sensitivities of the CO_2 front arrival times with respect to production/injection rates. The wells in the Brugge field are equipped with three inflow control valves (ICVs), with the first ICV completed in layers 1 and 2; the second ICV completed in layers 3, 4 and 5; and the third ICV completed in layers 6, 7, 8 and 9. The optimization is implemented by controlling the rates of the ICVs. Optimization was carried out in timestep of 6 months using norm weights of 0 and 10000.

The three different levels of constraints have been illustrated in **Fig. 3.11.** The Brugge field has 53 production ICVs and 30 injection ICVs. Comprehensive constraint matrices were set up for the field-scale optimization under following operational and facility constraints:

- Field production/injection rate ≤ 40000 RB/D
- Well and ICV production rate ≤ 3000 RB/D
- Well and ICV injection rate ≤ 4000 RB/D
- Production FBHP ≥ 740 Psia
- Injection FBHP ≤ 2626 Psia
- Water cut limit: 90%
- GOR limit: 100 Mscf/STB

The constraint matrices were updated dynamically to ensure that the above-mentioned constraints are satisfied at each hierarchical level during all time intervals.

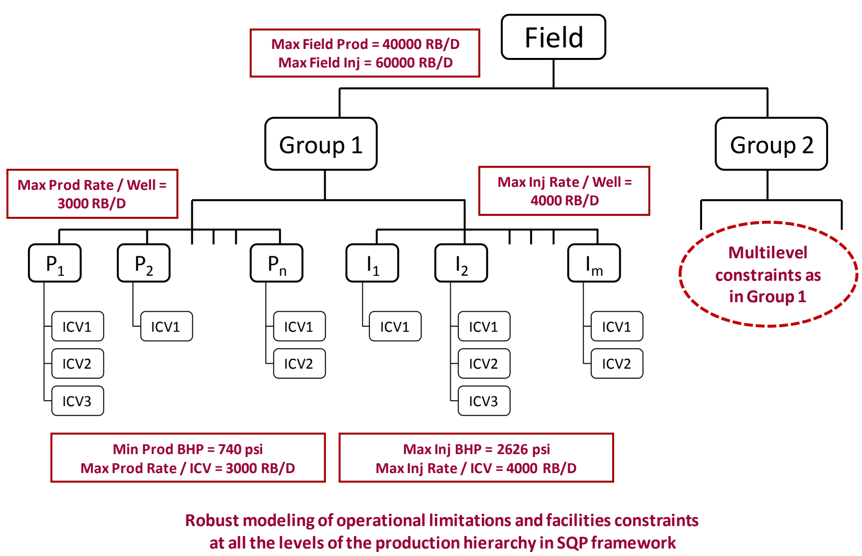

Fig. 3.11—Hierarchical production and facility related constraints considered for rate optimization.

3.4.1 CO_2 Flood Optimization Using Single Geologic Model

In this section we limit our optimization to a single geologic model. The impact of geological uncertainty will be discussed in the next example.

The base case considers reactive control where production/injection ICVs are operated at equal rates subject to constraints mentioned earlier. The production ICVs are shut as their water-cut exceeds 90% or GOR exceeds 100 Mscf/STB. We carried out rate optimization using norm weights of 0 and 10000 for the base case mentioned above. As shown in **Fig. 3.12a,** for injector 'BR-I6', ICVs–1, 2 and 3 operate at equal rates until injection FBHP for ICV–2 reaches the constraint specified. The cumulative CO_2 injection is thus similar for the three ICVs for base case (Fig. 3.12b). Sweep efficiency maximization (norm weight–0) allocates lower rates to ICV–2 and higher rates to ICV–3 **(Figs. 3.13a and 3.13b),** to improve areal sweep. As shown in **Figs. 3.14a and 3.14b,** the injection through ICV–3 increases further with acceleration. **Fig. 3.15** shows the permeability distribution from layers one to nine for index I–72 with well locations for 'BR-I6' and 'BR-P16'.

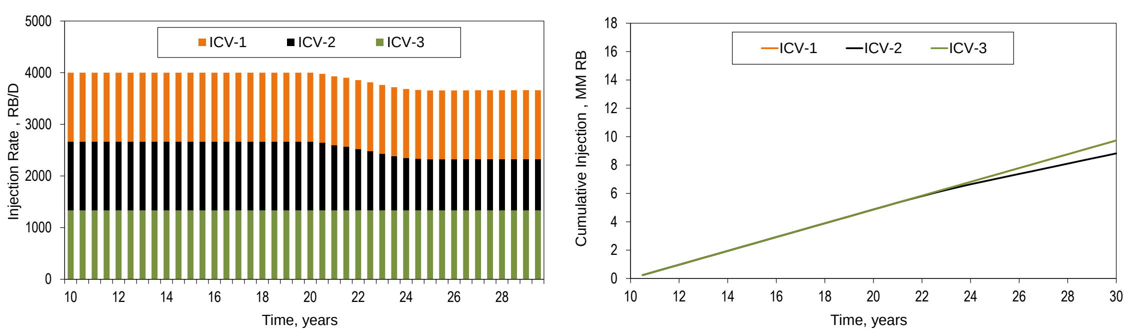

Fig. 3.12—(a) Voidage injection rate for ICVs–1, 2 and 3 of injector 'BR-I6' for base case (b) Cumulative voidage injection for respective ICVs.

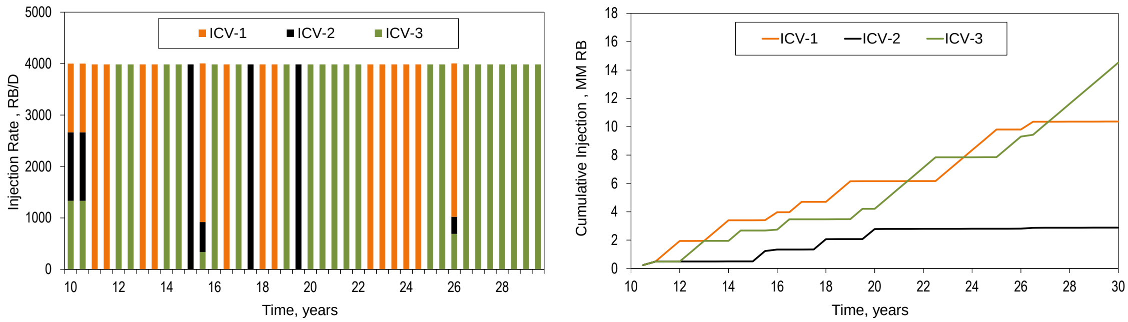

Fig. 3.13—(a) Voidage injection rate for ICVs–1, 2 and 3 of injector 'BR-I6' for sweep efficiency maximization (norm weight–0) (b) Cumulative voidage injection for respective ICVs.

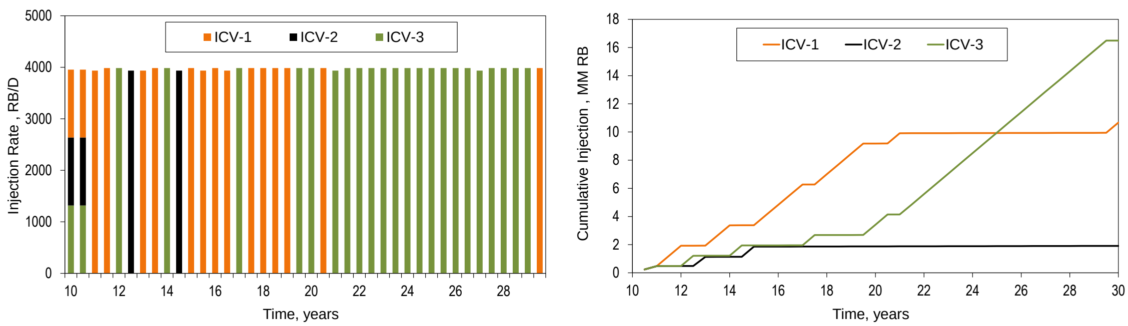

Fig. 3.14—(a) Voidage injection rate for ICVs–1, 2 and 3 of injector 'BR-I6' for production acceleration (norm weight–10000) (b) Cumulative voidage injection for respective ICVs.

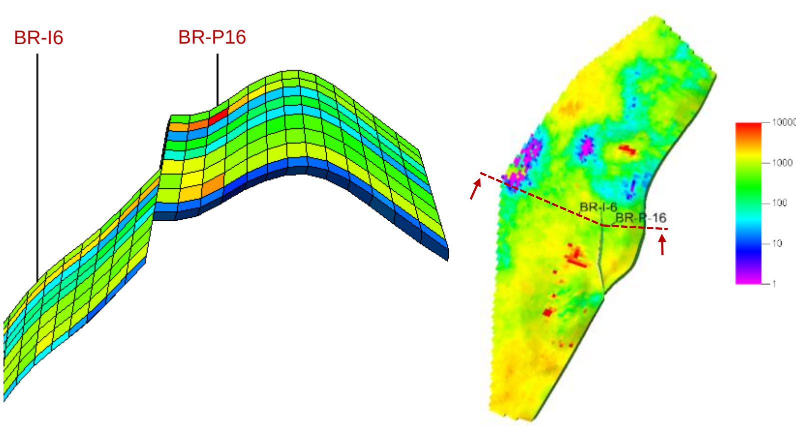

Fig. 3.15—Permeability distribution (layers 1 to 9) for index I–72.

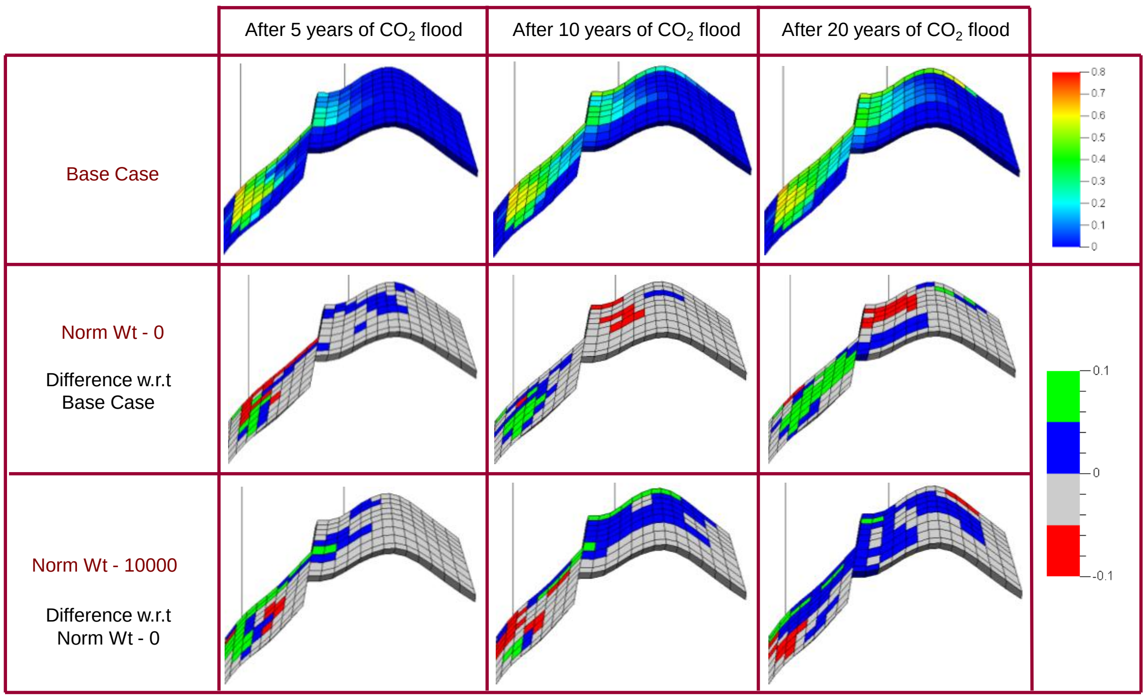

Fig. 3.16—Gas saturation along index I–72 after 5, 10 and 20 years of CO_2 flood for base case, sweep efficiency maximization (norm weight–0) and production acceleration (norm weight–10000).

The first row of **Fig. 3.16** shows the gas saturation along index I–72 for base case, which shows gravity segregation at different times. The CO_2 front lags behind for layers 3, 4 and 5 corresponding to ICV–2 owing to lower permeability and constrained injection at later times. The optimal rates corresponding to norm weight–0 result in higher gas saturation in layers 2 to 6 and better sweep of low permeability layers for I–72. Acceleration reduces gravity segregation and improves sweep further. The second row in **Fig. 3.17** shows the residual oil saturation for layer 2, 4 and 8 at the end of 20 years of CO_2 flood. As shown by third row of Fig. 3.17, the optimal rates corresponding to norm weight of 0 result in reduction of residual oil saturation at the end of CO_2 flood, owing to better sweep in all of the layers. The last row of Fig. 3.17 shows further reduction in oil saturation with production acceleration.

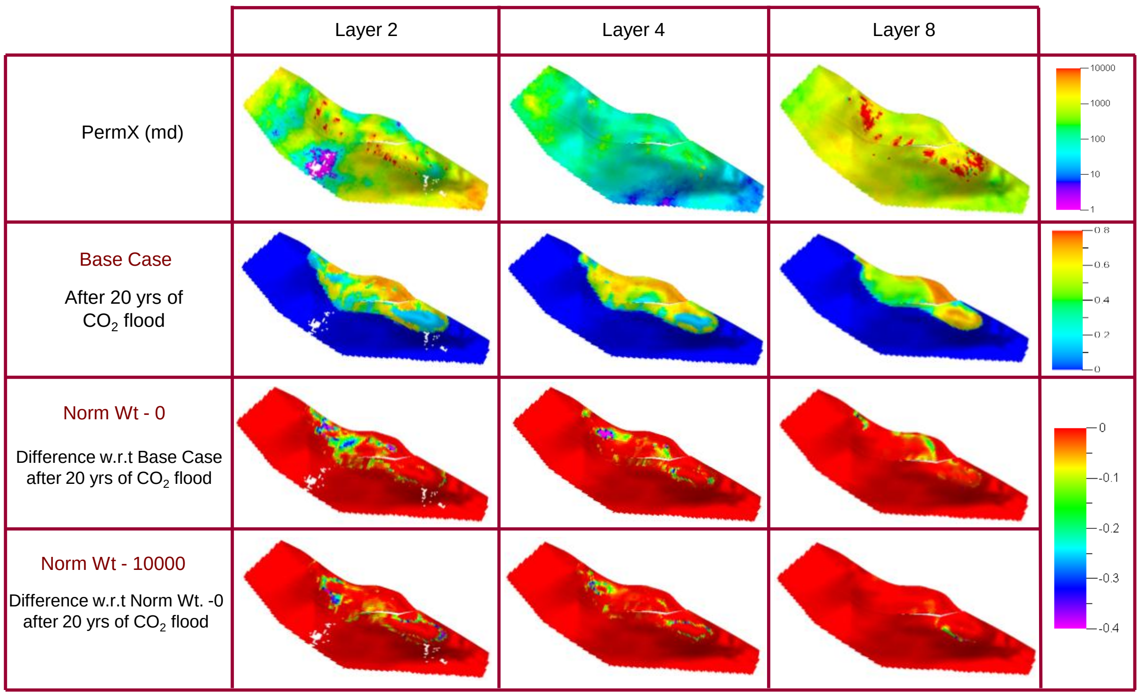

Fig. 3.17—Oil saturation after 20 years of CO_2 flood for base case, sweep efficiency maximization (norm weight–0) and production acceleration (norm weight–10000).

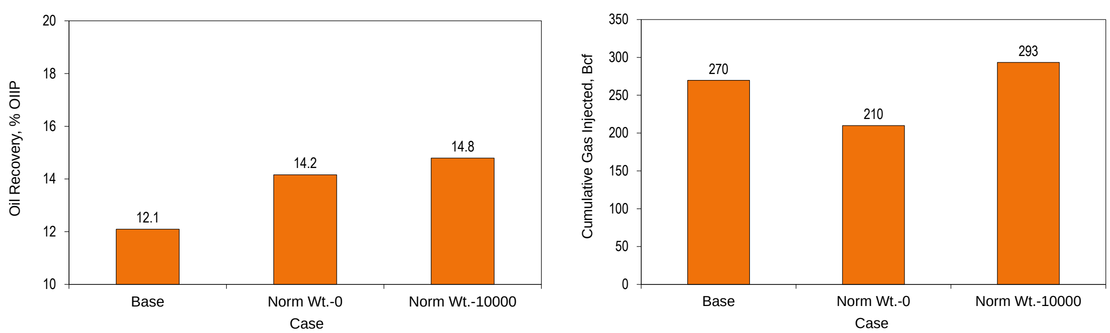

Fig. 3.18—(a) Incremental oil recovery (w.r.t OOIP) for 20 years of CO_2 flood for base case, sweep efficiency maximization (norm weight–0) and production acceleration (norm weight–10000). (b) Cumulative gas injection for respective cases.

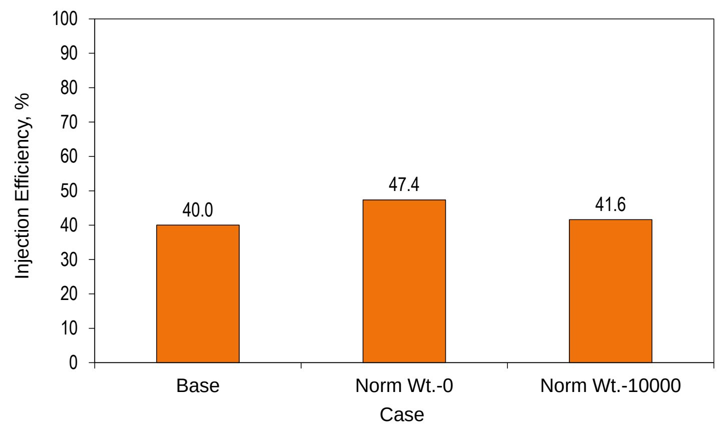

Fig. 3.19—Injection efficiency for base case, sweep efficiency maximization (norm weight–0) and production acceleration (norm weight–10000).

Fig. 3.18a shows the increase in 'incremental oil recovery' with rate optimization for norm weights of 0 and 10000. The recovery shown in the figure corresponds to production during later 20 years w.r.t. OIIP. It should be noted that cumulative CO_2 injected for sweep efficiency maximization (norm weight–0) is less compared to that for the base case (Fig. 3.18b). Acceleration (norm weight–10000) results in increase in oil recovery owing to improved VGR caused by higher CO_2 injection rates. The increase in injection efficiency with sweep efficiency maximization, as shown in **Fig. 3.19**, demonstrates the practical viability of our approach. Production acceleration, however, results in higher recovery at the expense of injection efficiency.

3.4.2 CO_2 Flood Optimization Using Multiple Models

In this section we incorporate geologic uncertainty into the optimization using multiple geologic realizations. A set of 104 realizations were generated based on the reservoir properties and well log attributes extracted from a high-resolution geologic model. History matching was implemented for 30 realizations by changing the permeability field using streamline-based generalized-travel-time inversion (Alhuthali et al. 2010).

The realization from the previous case was considered as reference realization. We considered 10 history matched realizations (including reference realization) of the

Brugge field for rate optimization. The optimization was carried out using the expected value formulation as discussed before, under risk neutral conditions (r–0). **Fig. 3.20** shows the permeability distribution in the top layer for each of the 10 realizations to illustrate variability amongst the realizations. The optimized rates thus obtained were applied to a blind realization which was not included in the optimization process. To illustrate the robustness of our approach, we applied to the same blind realization the optimal rates obtained from the single realization optimization as discussed in the previous section. For comparison purposes, the top layer permeability for the blind realization used to test the optimization methods is shown in Fig. **3.21**.

Fig. 3.22 compares the performance of the blind realization in terms of field GOR and oil recovery under two scenarios. The first scenario uses the rate derived from optimization of single realization (SR), whereas the second scenario accounts for geologic uncertainty based on the expected value of arrival time residuals from multiple realizations (MR). We used norm weight of 0 for both the scenarios.

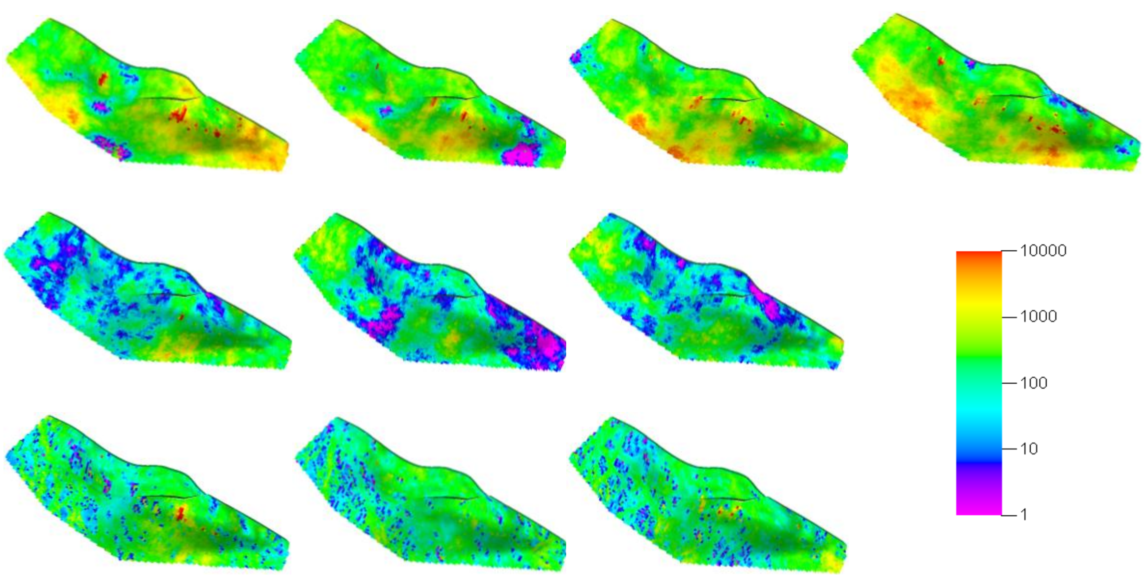

Fig. 3.20—Permeability (layer 1) for 10 history matched realizations used in stochastic optimization.

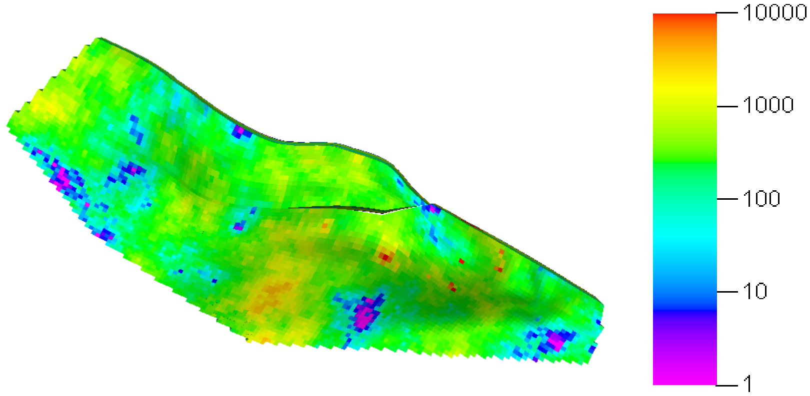

Fig. 3.21—Permeability (layer 1) for blind realization.

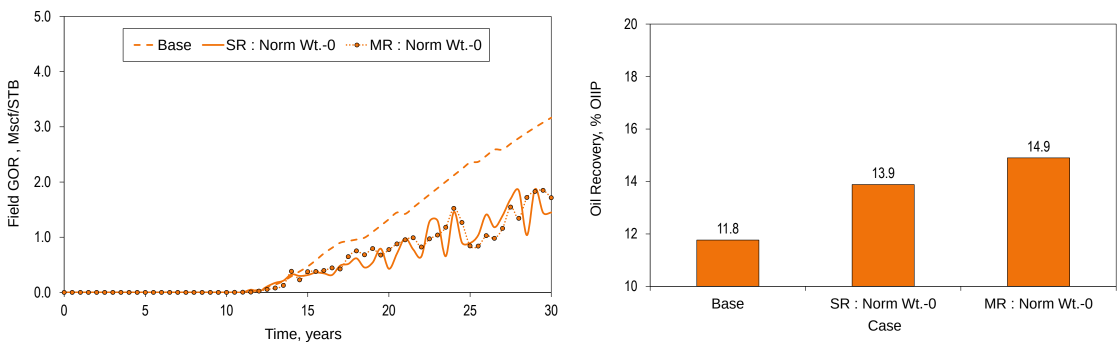

Fig. 3.22—(a) Field GOR for base case and sweep efficiency maximization (norm weight–0) for rate optimization of single realization (SR) and multiple realizations (MR) (b) Incremental oil recovery (w.r.t OOIP) for 20 years of CO_2 flood for respective cases.

The optimal rates corresponding to MR optimization resulted in higher oil recovery and higher injection efficiency **(Fig. 3.23)** over SR optimization, when applied to the blind realization. The results clearly demonstrate the ability of our approach to address geologic uncertainty during field-scale flood optimization.

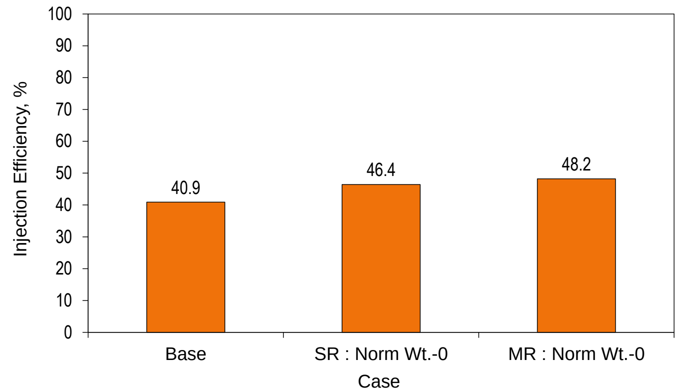

Fig. 3.23—Injection efficiency for base case and sweep efficiency maximization (norm weight–0) for rate optimization of single realization (SR) and multiple realizations (MR).

3.4.3 WAG Flood Optimization Using Single Geologic Model

In this section we illustrate the application of our approach for WAG flooding using the reference realization.

The base case considers alternate injection of water and CO_2 for 4 months and 2 months respectively under reactive control described earlier. This results in WAG ratio (volume water/volume CO_2 at reservoir condition) of 2:1 during each cycle **(Fig. 3.24a).**

The optimal production/injection rates for maximizing sweep efficiency were obtained using norm weight of 0. The average WAG ratio for 20 years of production for sweep efficiency maximization is close to that for the base case. However, as shown in Fig. 3.24b, the WAG ratio for each cycle varies from 1.2 RB/RB to 3.9 RB/RB. Acceleration corresponding to norm weight of 10000 causes the injection rate, for both water and CO_2, to approach the upper limit. This results in WAG ratio of 2:1 for most of the WAG cycles during acceleration. The effects of rate optimization on field water cut and GOR are shown in **Figs. 3.25a and 3.25b.** The optimal rates for maximizing sweep efficiency result in delayed CO_2 breakthrough and reduced water and CO_2 recycling. However, the production/injection rates increase with acceleration resulting in higher field water cut and GOR.

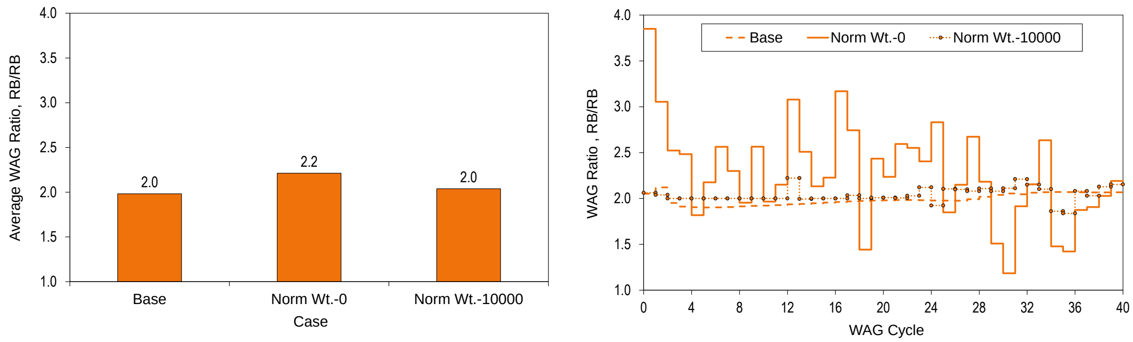

Fig. 3.24—(a) Average WAG ratio for 20 years of WAG flood for base case, sweep efficiency maximization (norm weight–0) and production acceleration (norm weight–10000). (b) WAG ratio for 6 months cycle for respective cases.

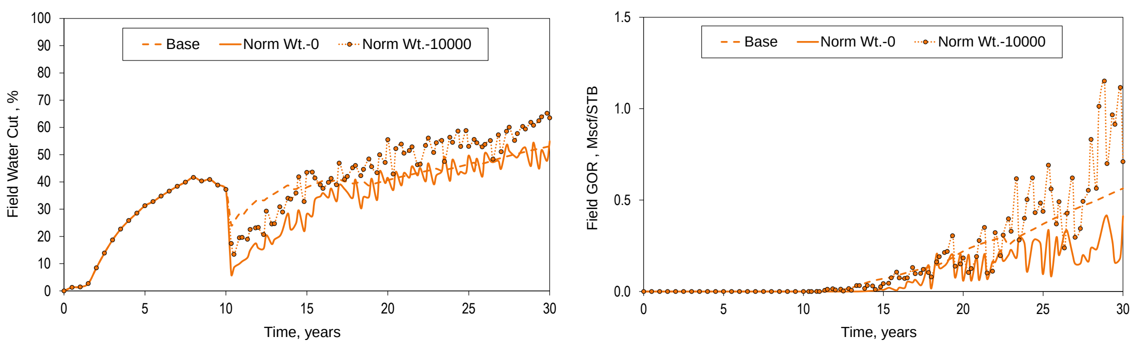

Fig. 3.25—(a) Field water cut during WAG flood for base case, sweep efficiency maximization (norm weight–0) and production acceleration (norm weight–10000). (b) Field GOR for respective cases.

Fig. 3.26 shows the increase in 'incremental oil recovery' with rate optimization for norm weights of 0 and 10000. The cumulative water and CO_2 injected for maximizing sweep efficiency is less compared to that for the base case **(Figs. 3.27a and 3.27b).** Acceleration results in increase in oil recovery owing to improved VGR caused by higher water and CO_2 injection rates. Finally, from **Fig. 3.28** we can see that sweep efficiency maximization improves injection efficiency, which further decreases with increase in norm weight. The results clearly demonstrate the potential and practical viability of our approach.

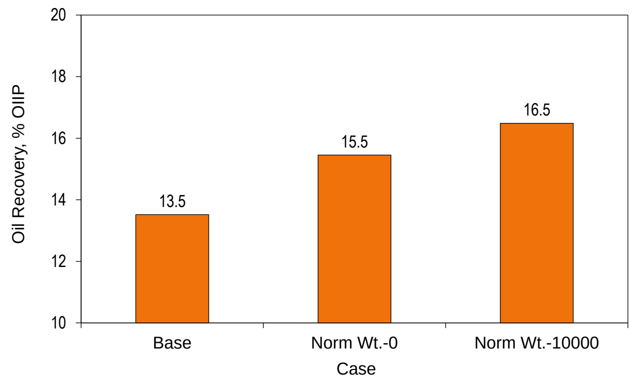

Fig. 3.26—Incremental oil recovery (w.r.t OOIP) for 20 years of WAG flood for base case, sweep efficiency maximization (norm weight–0) and production acceleration (norm weight–10000).

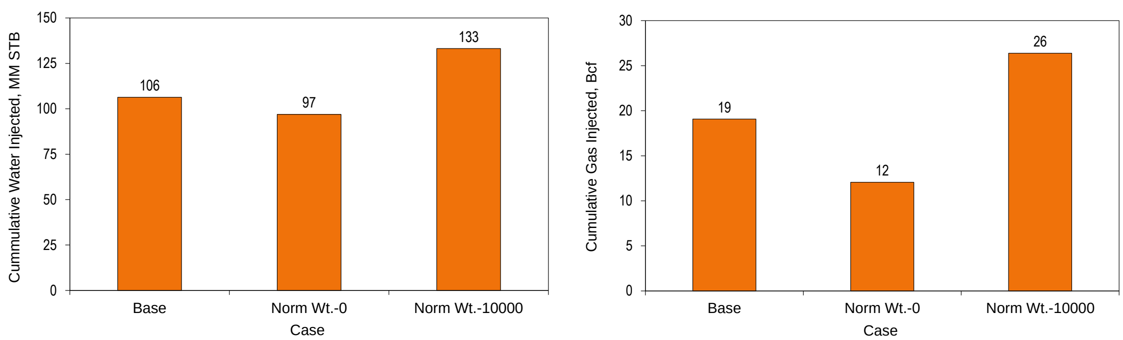

Fig. 3.27—(a) Cumulative water injected during WAG flood for base case, sweep efficiency maximization (norm weight–0) and production acceleration (norm weight–10000). (b) Cumulative gas injection for respective cases.

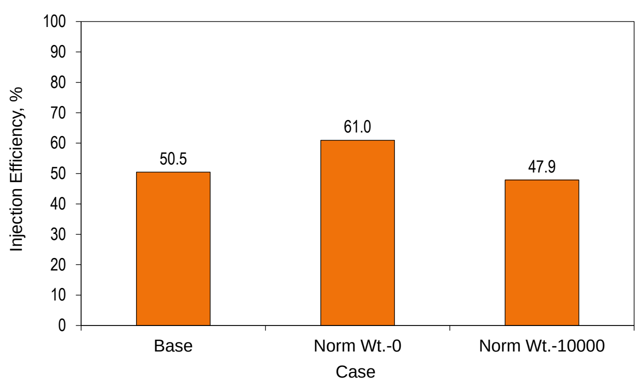

Fig. 3.28—Injection efficiency during WAG flood for base case, sweep efficiency maximization (norm weight–0) and production acceleration (norm weight–10000).

3.5 Summary

In this chapter, we demonstrated an efficient approach for optimizing CO_2 flood via rate control. The approach relies on making an optimal decision based on a compromise between maximizing sweep efficiency and accelerating production. Because of analytical computation of the sensitivities and the gradient and Hessian of the objective function, the approach is computationally efficient and suitable for large field cases. The hierarchy of rate and pressure constraints is captured during optimization through comprehensive constraint matrices. Moreover, the approach can account for geologic uncertainty using multiple realizations via a stochastic optimization framework.

The applicability and robustness of the approach has been demonstrated using 3D synthetic example, the Brugge field. Significant improvement in oil recovery and reduction in CO_2 recycling was achieved over base case with rate optimization. Geologic uncertainty was addressed using 10 history matched realizations for optimization and applying the rates derived from optimization to a blind realization. Results showed that the optimal rates significantly improve sweep efficiency and oil recovery over base case. Finally, the approach was used to improve sweep during WAG flood which resulted in significant improvement in oil recovery and reduction in water and CO_2 recycling.

CHAPTER IV

CONCLUSIONS

The presence of reservoir heterogeneity, geological uncertainty and complex displacement mechanisms involved in EOR processes like polymerflood, CO_2 flood etc. underscores the need for a prudent reservoir management with an objective to maximize sweep. This can be achieved by optimal selection of production/injection rates under field production and facility related constraints. The increasing deployment of smart well completions and i-field has inspired many researchers to develop algorithms to optimize the production/injection rates along intervals of smart wells. These algorithms have been successfully tested and applied to field-scale problems for waterflooding. However, the application of rate control for other EOR methods has been relatively few and far between.

The primary objective of our approach is to improve sweep during polymerflood and CO_2 flood by equalizing flood front arrival time at multiple producers. We trace streamlines using the fluid fluxes derived from the finite-difference flow simulation. The streamlines are then used to analytically compute the sensitivities and the gradient and Hessian of the objective function. The hierarchy of rate and pressure constraints is captured during optimization through comprehensive constraint matrices. The objective function is then minimized using Sequential Quadratic Programming technique to generate required changes in rates subject to specified field constraints. Moreover, the approach can account for geologic uncertainty using multiple realizations via a stochastic optimization framework. Following conclusions can be made based on this study:

- Streamline time-of-flight can be effectively used to optimize EOR processes like polymerflood, CO_2 flood etc. through equalizing the front arrival time at the producers. This results in increased cumulative oil production improved injection efficiency.

- The effect of polymer/CO_2 breakthrough is incorporated into the objective function by rescaling the original arrival time, to allocate lower rate to wells recycling polymer/CO_2 as compared to other wells. This allows for optimization after breakthrough at a well and reduction in recycling of injected phase.
- An accelerated production strategy with higher NPV can be obtained by optimal selection of norm weight. Increase in norm weight results in high VGR and thereby reduced gravity segregation during CO_2 flood.
- Optimal production/injection rates can be obtained to improve sweep and increase oil recovery for water-alternate-CO_2 flood.
- Because of analytical computation of the sensitivities and the gradient and Hessian of the objective function, the approach is computationally efficient as it requires only one simulation per iteration per realization. This makes it suitable for large field cases.
- The hierarchy of rate and pressure constraints is captured during optimization through comprehensive constraint matrices. These constraint matrices are updated dynamically to ensure that the specified constraints are honored at each hierarchical level during all time intervals. This makes it applicable to real field scenarios.
- Geological uncertainty is addressed in terms of a stochastic form of objective function which includes the expected value and the standard deviation combined with a risk coefficient, making the approach robust.
- We show that the approach yields robust rates for polymerflooding using a field-scale example from Goldsmith San Andres Unit (GSAU). Significant improvement in oil recovery and reduction in polymer recycling was achieved over the base case with the application of rate optimization. Geologic uncertainty was addressed using 10 history matched realizations for

optimization and applying the rates derived from optimization to a blind realization. The applicability and robustness of the approach for CO_2 flooding has been demonstrated using 3D synthetic example, the Brugge field. Significant improvement in oil recovery and reduction in CO_2 recycling was achieved over base case with rate optimization. Geologic uncertainty was addressed using 10 history matched realizations for optimization and applying the rates derived from optimization to a blind realization. Results showed that the optimal rates significantly improve sweep efficiency and oil recovery over base case. Finally, the approach was used to improve sweep during WAG flood which resulted in significant improvement in oil recovery and reduction in water and CO_2 recycling.

NOMENCLATURE

e	Arrival time residual vector, t, day(s)
E	Expected value
f_{gas}	Ratio of produced GOR to maximum allowable GOR limit, dimensionless, frac.
f_{pol}	Ratio of polymer produced to maximum allowable production limit, dimensionless, frac.
f_w	Water cut, dimensionless, frac.
$f(\mathbf{q})$	Scalar objective function, t^2, sq day(s)
$\mathbf{g(q)}$	Inequality constraints, L^3/t, B/D [m^3/d]
$\mathbf{h(q)}$	Equality constraints, L^3/t, B/D [m^3/d]
g	Acceleration due to gravity, L/t^2, ft/s^2 [m/s^2]
i, j	Well index
k_v	Geometric mean of permeability, L^2, md
m	Group index
$N_{prod,m}$	Number of production well(s) in group *m*
N_{group}	Number of group(s)
$p(\mathbf{q})$	Scalar objective function, t^2, sq day
$\mathbf{q}$	Total fluid rate vector, L^3/t, B/D [m^3/d]
r	Risk coefficient, dimensionless
S_{ij}	Sensitivities coefficient, t^2/L^3, sq D/B [s^2/m^3]
t	Arrival time vector, t, day(s)
$t_{i,m}$	Arrival time at producer *i* which belongs to group *m*, t, day(s)
$t_{d,m}$	Desired arrival time for group *m*, t, day(s)
z	Geologic realization index
$\bar{v}$	Average Darcy velocity, L/t, ft/day [m/d]
α	Exponent term, dimensionless
$\Delta\mu$	Viscosity difference between oil and CO_2, m/Lt, cp [Pa.s]

$\Delta\rho$	Density difference between oil and CO_2, m/L^3, lbm/ft^3 [kg/m^3]
η	Norm weight, dimensionless
λ_K	Karush-Kuhn-Tucker multipliers for inequality constraints
λ_L	Lagrange multipliers for equality constraints
σ	Standard deviation

REFERENCES

Alhuthali, A.H., Oyerinde, D. and Datta-Gupta, A. 2007. Optimal Waterflood Management Using Rate Control. *SPE Res Eval & Eng* **10** (5): 539–551. SPE-102478-PA. doi: 10.2118/102478-PA.

Alhuthali, A.H., Datta-Gupta, A., Yuen, B. and Fontanilla, J.P. 2008. Optimal Rate Control Under Geologic Uncertainty. Paper SPE 113628 presented at the SPE/DOE Symposium on Improved Oil Recovery, Tulsa, Oklahoma, USA, 20–23 April. doi: 10.2118/113628-MS.

Alhuthali, A.H., Datta-Gupta, A., Yuen, B. and Fontanilla, J.P. 2010. Field Applications of Waterflood Optimization via Optimal Rate Control With Smart Wells. *SPE Res Eval & Eng* **13** (3): 406–422. SPE-118948-PA. doi: 10.2118/118948-PA.

Brouwer, D.R. and Jansen, J.D. 2004. Dynamic Optimization of Water Flooding with Smart Wells Using Optimal Control Theory. *SPE J.* **9** (4): 391–402. SPE-78278-PA. doi: 10.2118/78278-PA.

Caudle, B.H. and Dyes, A.B. 1958. Improving Miscible Displacement by Gas-Water Injection. *Trans.*, AIME, **213:** 281–283.

Christie, M.A. and Bond, D.J. 1987. Detailed Simulation of Unstable Processes in Miscible Flooding. *SPE Res Eng* **2** (4): 514–522. SPE-14896-PA. doi: 10.2118/14896-PA.

Clemens, T., Abdev, J. and Thiele, M. 2010. Improved Polymer-Flood Management Using Streamlines. Paper SPE 132774 presented at the SPE Annual Technical Conference and Exhibition, Florence, Italy, 19–22 September. doi: 10.2118/132774-MS.

Craig, F.F. Jr. 1993. *The Reservoir Engineering Aspects of Waterflooding*. Monograph Series, SPE, Richardson, Texas **3.**

Craig, F.F. Jr., Sanderlin, J.L., Moore, D.W. and Geffen, T.M. 1957. A Laboratory Study of Gravity Segregation in Frontal Drives. *Trans.*, AIME, **210:** 275–282.

Datta-Gupta, A. and King, M.J. 2007. *Streamline Simulation: Theory and Practice*. Textbook Series, SPE, Richardson, Texas **11.**

ECLIPSE©, Version 2010.2. 2010. Houston, Texas: Schlumberger Information Solutions.

Fayers, F.J. and Muggeridge, A.H. 1990. Extensions to Dietz Theory and Behavior of Gravity Tongues in Slightly Tilted Reservoirs. *SPE Res Eng* **5** (4): 487–494. SPE-18438-PA. doi: 10.2118/18438-PA.

Fayers, F.J., Blunt, M.J. and Christie, M.A. 1992. Comparisons of Empirical Viscous-Fingering Models and Their Calibration for Heterogeneous Problems. *SPE Res Eng* **7** (2): 195–203. SPE-22184-PA. doi: 10.2118/22184-PA.

Green, D.W. and Willhite, G.P. 1998. *Enhanced Oil Recovery*. Textbook Series, SPE, Richardson, Texas **6**.

Habermann, B. 1960. The Efficiency of Miscible Displacement as a Function of Mobility Ratio. *Trans.*, AIME, **219:** 264–272.

Holm, L.W. and Josendal, V.A. 1974. Mechanisms of Oil Displacement by Carbon Dioxide. *J Pet Technol* **26** (12): 1427–1438. SPE-4736-PA. doi: 10.2118/4736-PA.

Jarrell, P.M., Fox, C., Stein, M. and Webb, S. 2002. *Practical Aspects of CO_2 Flooding*. Monograph Series, SPE, Richardson, Texas **22**.

Jasek, D.E., Frank, J.R., Mathis, L.S. and Smith, D.J. 1998. Goldsmith San Andres Unit CO_2 Pilot - Design, Implementation, and Early Performance. Paper SPE 48945 presented at the SPE Annual Technical Conference and Exhibition, New Orleans, Louisiana, 27–30 September. doi: 10.2118/48945-MS.

Jenkins, M.K. 1984. An Analytical Model for Water/Gas Miscible Displacements. Paper SPE 12632 presented at the SPE Enhanced Oil Recovery Symposium, Tulsa, Oklahoma, 15–18 April. doi: 10.2118/12632-MS.

Jimenez, E.A., Datta-Gupta, A. and King, M.J. 2008. Full Field Streamline Tracing in Complex Faulted Systems with Non-Neighbor Connections. Paper SPE 113425 presented at the SPE/DOE Symposium on Improved Oil Recovery, Tulsa, Oklahoma, USA, 20–23 April. doi: 10.2118/113425-MS.

Kaminsky, R.D., Wattenbarger, R.C., Szafranski, R.C. and Coutee, A.S. 2007. Guidelines for Polymer Flooding Evaluation and Development. Paper IPTC 11200 presented at the International Petroleum Technology Conference, Dubai, U.A.E., 4–6 December. doi: 10.2523/11200-MS.

Koval, E.J. 1963. A Method for Predicting the Performance of Unstable Miscible Displacement in Heterogeneous Media. *SPE J.* **3** (2): 145–154. SPE-450-PA. doi: 10.2118/450-PA.

Lake, L.W. 1989. *Enhanced Oil Recovery*. Englewood Cliffs, New Jersey: Prentice Hall.

Lake L W., Schmidt R. L. and Venuto P. B. 1992. A Niche for Enhanced Oil Recovery in the 1990s. *Oilfield Review* **4** (1): 55–61.

MATLAB®, Version 7.11.0. 2010. Natick, Massachusetts: The MathWorks, Inc.

Moritis, G. 2008. Worldwide EOR Survey. *Oil Gas J.* **106:** 41–59.

Nocedal, J. and Wright, S.J. 2006. *Numerical Optimization*, 2nd ed. New York: Springer Science + Buisness Media.

Peters, L., Arts, R.J., Brouwer, G.K., Geel, C.R., Cullick, S., Lorentzen, R.J., Chen, Y. et al. 2010. Results of the Brugge Benchmark Study for Flooding Optimization and History Matching. *SPE Res Eval & Eng* **13** (3): 391–405. SPE-119094-PA. doi: 10.2118/119094-PA.

Rossen, W.R., van Duijn, C.J., Nguyen, Q.P., Shen, C. and Vikingstad, A.K. 2010. Injection Strategies to Overcome Gravity Segregation in Simultaneous Gas and Water Injection into Homogeneous Reservoirs. *SPE J.* **15** (1): 76–90. SPE-99794-PA. doi: 10.2118/99794-PA.

Sorbie, K.S. 1991. *Polymer-Improved Oil Recovery*. London: Blackie and Son Ltd.

Spivak, A. 1974. Gravity Segregation in Two-Phase Displacement Processes. *SPE J.* **14** (6): 619–632. SPE-4630-PA. doi: 10.2118/4630-PA.

Stalkup, F.I. 1983. *Miscible Displacement*. Monograph Series, SPE, Richardson, Texas **8**.

Stone, H.L. 1982. Vertical Conformance in an Alternating Water-Miscible Gas Flood. Paper SPE 11130 presented at the SPE Annual Technical Conference and Exhibition, New Orleans, Louisiana, 26–29 September. doi: 10.2118/11130-MS.

Sudaryanto, B. and Yortsos, Y.C. 2001. Optimization of Displacements in Porous Media Using Rate Control. Paper SPE 71509 presented at the SPE Annual Technical Conference and Exhibition, New Orleans, Louisiana, 30 September–3 October. doi: 10.2118/71509-MS.

Tavakkolian, M., Jalali F., F. and Emadi, M.A. 2004. Production Optimization Using Genetic Algorithm Approach. Paper SPE 88901 presented at the Nigeria Annual International Conference and Exhibition, Abuja, Nigeria, 2–4 August. doi: 10.2118/88901-MS.

Taware, S., Sharma, M. and Datta-Gupta, A. 2010. Optimal Water Flood Management Under Geological Uncertainty Using Accelerated Production Strategy. Paper SPE 133882 presented at the SPE Annual Technical Conference and Exhibition, Florence, Italy, 19–22 September. doi: 10.2118/133882-MS.

Tchelepi, H.A. and Orr, F.M. Jr. 1994. Interaction of Viscous Fingering, Permeability Heterogeneity, and Gravity Segregation in Three Dimensions. *SPE Res Eng* **9** (4): 266–271. SPE-25235-PA. doi: 10.2118/25235-PA.

Todd, M.R. and Longstaff, W.J. 1972. The Development, Testing, and Application of a Numerical Simulator for Predicting Miscible Flood Performance. *J Pet Technol* **24** (7): 874–882. SPE-3484-PA. doi: 10.2118/3484-PA.

Wang, D., Seright, R.S., Shao, Z. and Wang, J. 2008. Key Aspects of Project Design for Polymer Flooding at the Daqing Oilfield. *SPE Res Eval & Eng* **11** (6): 1117–1124. SPE-109682-PA. doi: 10.2118/109682-PA.

VITA

Name	Mohan Sharma
Address	c/o Dr. Akhil Datta-Gupta
	3116 TAMU, RICH-702
	Dept. of Petroleum Engineering
	Texas A&M University, College Station
	TX - 77843
Email Address	mohansharma17@gmail.com

Education	B.S., Petroleum Engineering, Indian School of Mines,
	Dhanbad, India, 2006
	M.S., Petroleum Engineering, Texas A&M University,
	College Station, 2011
Experience	Production Engineer, BG EPIL, 2006-2007
	Reservoir Engineer, BG EPIL, 2007-2009